

Weakly correlated electrons on a square lattice: a renormalization group theory

D. Zanchi

Institut für Theoretische Physik der Freien Universität Berlin, Arnimallee 14, 14195 Berlin, Germany

and

Laboratoire de Physique Théorique et Hautes Energies. Universités Paris VI Pierre et Marie Curie – Paris VII Denis

*Diderot, 2 Place Jussieu, 75252 Paris Cédex 05, France. **

H. J. Schulz[†]

Laboratoire de Physique des Solides, Université Paris-Sud, 91405 Orsay, France

We formulate the exact Wilsonian renormalization group for a system of interacting fermions on a lattice. The flow equations for all vertices of the Wilson effective action are expressed in form of the Polchinski equation. We apply this method to the Hubbard model on a square lattice using both zero- and finite-temperature methods. Truncating the effective action at the sixth term in fermionic variables we obtain the one-loop functional renormalization equations for the effective interaction. We find the temperature of the instability T_c^{RG} as function of doping. We calculate furthermore the renormalization of the angle-resolved correlation functions for the superconductivity (SC) and for the antiferromagnetism (AF). The dominant component of the SC correlations is of the type $d_{x^2-y^2}$ while the AF fluctuations are of the type s . Following the strength of both SC and AF fluctuation along the instability line we obtain the phase diagram. The temperature T_c^{RG} can be identified with the crossover temperature T_{co} found in the underdoped regime of the high-temperature superconductors, while in the overdoped regime T_c^{RG} corresponds to the superconducting critical temperature.

74.20.Mn, 74.25.Dw, 75.30.Fv

PAR/LPTHE/98-60

December 1998

^{*}present address

[†]deceased

I. INTRODUCTION

In systems of correlated fermions on a lattice some interesting and also puzzling physics seems to happen when interaction-induced localization tendencies, antiferromagnetic, and superconducting fluctuations get mixed. The standard example of such a system are the copper–oxide superconductors.¹ In the underdoped regime, between the AF and SC phases, correlations of both AF and SC type are strongly enhanced, and a pseudogap is visible in the one particle spectrum and in the spin response functions. The pseudogap regime is limited from above by a crossover temperature $T_{co}(x)$, a monotonously decreasing function of doping. At the temperatures $T \gtrsim T_{co}$ the underdoped materials are “strange metals”: many physical properties are unlike those of a standard Fermi liquid². In the overdoped regime $T_{co}(x)$ merges with the critical temperature for superconductivity and the regime $T > T_c$ is merely a Fermi liquid. Another interesting feature of the phase diagram is the unusual form of the order parameter. After a rather long period of controversies the $d_{x^2-y^2}$ –symmetry is finally generally accepted.³ This is one of the reasons to believe that the pairing mechanisms are tightly related to the antiferromagnetic tendencies and not to the standard phonon–exchange mechanisms. The $d_{x^2-y^2}$ –form of the superconducting correlations subsists also in the pseudogap regime as is seen in recent angle–resolved photoemission⁴ and tunneling⁵ experiments. The simultaneous existence of strong AF correlations, as seen by NMR⁶ or neutron–scattering⁷ experiments, and even localization tendencies as flattening of the band⁸ make us conclude that the interpretation of this regime only terms of superconducting or antiferromagnetic fluctuations only is not sufficient, especially because we expect that they are coupled.

It is striking that some other apparently completely different systems of correlated fermions have very similar properties. A phase diagram with the superconducting phase in the vicinity of the spin density wave (i.e. antiferromagnetic) instability characterizes also the quasi–one–dimensional Bechgaard salts⁹ and the quasi–two–dimensional organic superconductors of the ET family,¹⁰ where instead of doping the relevant parameter for the phase diagram is pressure. However the common feature of all these compounds is that they are systems of correlated fermions with reduced dimensionality ($D < 3$) and with strongly anisotropic and more or less nested Fermi surfaces. The main points for the understanding of the three groups of compounds are: (i) the destruction of the nesting by doping (cuprates) or by applying pressure (Bechgaard salts and ET); (ii) the suppression of the Umklapp processes by doping the the half-filled band (in the cuprates and ET-s) or by making the half-filled band effectively quarter-filled through the breaking the longitudinal dimerization by pressure (in the Bechgaard salts). Concerning the Bechgaard salts it is interesting to remark that some very recent interpretations of the phase diagram of the (TMTSF)PF₆ material¹¹ suggest that the intermediate regime between the high–temperature 1D behavior and the low temperature 3D physics is a strange 2D–liquid with properties very similar to those of the underdoped cuprates above the crossover temperature T_{co} .

From the theoretical point of view it is certainly interesting to construct a theory able to treat on the same footing antiferromagnetic and superconducting tendencies in more than one dimension and to follow how the result changes with some external parameter that destroys nesting and the Mott–like localization. The first question one can ask is whether a purely repulsive model like for example the Hubbard model (or some generalization of it)

contains the coexisting and inter-depending antiferromagnetic and superconducting correlations. In such a model the antiferromagnetic fluctuations are associated with the enhancement of the particle-hole (p-h) propagators at low energies and the superconducting tendencies appear through particle-particle (p-p) propagators. The Hubbard model is appropriate because at half filling already a simple mean-field calculation gives an antiferromagnetic instability at a finite temperature. However if one tries to include also the p-p processes already in the weak coupling limit the problem becomes nontrivial already in the weak coupling limit: a simple mean-field theory is not able to follow both p-h and p-p correlation channels. One can of course try to remedy this problem by including summation of selected subseries of higher-order diagrams. One such attempt was to calculate the effective Cooper amplitude as a sum of bubble and ladder RPA series^{12,13}. The resulting Cooper amplitude is then used as coupling constant for assumed effective BCS theory. This procedure thus explicitly decouples three different summations (RPA bubbles, RPA ladder, and BCS ladder) without real justification. The FLEX (conserving) calculations¹⁴ based on the similar simplifications are also prejudiced by the choice of diagrams to be summed. The only way to proceed systematically is to construct the renormalization group that takes into account all p-p and p-h loops of a given order (or to use the equivalent parquet approach). In (quasi-) one dimension the renormalization group has been successfully used and is one of the basic theoretical ingredients in the physics of low-dimensional metals^{9,15,16}.

In two dimensions only a limited number of simplified cases was solved by the renormalization group. The poor man's scaling applied only to the interactions between electrons placed at the van Hove points it gives an antiferromagnetic instability at half-filling and superconductivity of $d_{x^2-y^2}$ symmetry if the deviation of the chemical potential μ from its value at half-filling becomes of the order of critical temperature of the antiferromagnetic state.¹⁷ The equivalent parquet approach has been used for half-filling (but without the limitation to the van Hove points) and also finds an antiferromagnetic instability.^{18,19} Parquet calculations for simple flat Fermi surfaces²⁰ give an antiferromagnetic instability but can not provide a continuous phase diagram as function of some imperfect nesting parameter or band filling: the $d_{x^2-y^2}$ -like superconducting pole appears simply by cutting the p-h part of the flow, as in ref. 17. The scaling approach to a system with a Fermi surface with both flat and curved parts²¹ has also reported a superconducting instability in a purely repulsive model, together with deviations from Fermi liquid behavior. However, the complete one-loop renormalization group (or parquet) for the real *band* of electrons with imperfect and tunable nesting, or doping, still remains unresolved. The main difficulty is related to the correct treatment of the coupling between p-p and p-h channels.

Different authors have tried to avoid to take into account the coupling between the different renormalization channels making drastic simplifications or limiting themselves to some particular forms of the Fermi surfaces or only to the low energy effective action. In our former publications^{22,23} we have shown that in the Hubbard model one can treat the p-h channel perturbatively if the filling is sufficiently far from one half. Then the renormalization group gives only a weak Kohn-Luttinger like pairing. The p-p part of the flow is decoupled from the p-h one in the low energy regime for the simple reason that the p-h part is negligible there. Other calculations based on the perturbative treatment of the p-h channel were also reported.^{24,25} If the Fermi surface is well (but imperfectly) nested, and this is exactly the interesting regime, this strategy does not work any more because both p-p and p-h loops are non-perturbatively large,

even for weak interactions. In the case of the square Fermi surface (with or without the van Hove singularities) taking only the leading logarithmic part the coupling between the channels into account²⁶ is equally insufficient. Another way to proceed is to see the 2D Hubbard system as an ensemble of coupled chains:²⁷ this approach gives a phase diagram with superconductivity formed by pairs of electrons on different chains, giving rise to a spatially anisotropic version of an d -wave order parameter. Among the number of the theoretical approaches to the Hubbard model other than via the loop–summations the Monte Carlo calculations take in principle “everything” into account but it is still unclear whether they give²⁸ or not^{13,29} the superconductivity.

In the present paper we search to reliably determine the phase diagram of the Hubbard model in the vicinity of half–filling where p–h processes are non–perturbatively enhanced and at least nearly as important as p–p ones. We also detect the dominant components of the angle–resolved correlation functions for antiferromagnetism and superconductivity as function of temperature. This allows us to know the symmetry of the microscopic fields whose fluctuations become important. The method that we will use is a generalization of Shankar’s renormalization–group approach³⁰ to an arbitrary form of the Fermi surface. In particular, the Kadanoff–Wilson mode elimination (developed by Shankar for 2D fermions) applied to the effective action with only two–particles interaction keeps only the strictly logarithmic contributions to the flow. Thus even if the nesting is very good but not perfect the p–h part of the flow would be zero because the logarithmic singularity is destroyed by imperfect nesting. To keep the p–h part of the flow finite even in the case of imperfect nesting we start by formulating the *exact* Kadanoff–Wilson–Polchinski renormalization group for fermions on a lattice. It was formulated previously^{31,32} only for the quantum fields with *one* zero–energy point in the momentum space, like the ϕ^4 field theory (critical phenomena). In many–fermions system in more than one dimension we have on the contrary the whole Fermi surface that plays the role of the zero energy manifold, what makes the calculations more complicated. Starting with the full bandwidth as the initial energy cutoff we perform iterative mode elimination reducing the cutoff Λ around the Fermi surface. Collecting at each step of the renormalization all the terms (cumulants) of the effective action we obtain the Polchinski equation for the vertices of the effective theory at the given step of the renormalization. It is important that even if the initial interaction was only a four–point function (two–particle interaction) vertices of *all* higher orders are created by the renormalization procedure. Once the exact renormalization group is formulated we proceed with its truncation at the one–loop level: the one–loop truncation of the flow for the four–point vertex is done by neglecting all renormalization–group–created vertices of order larger than six. Shankar³⁰ already has remarked that the six–point function created by the mode elimination is essential to get non–logarithmic contribution to the four point vertex (the effective interaction). The one–loop renormalization of the interaction that we obtain in this way appears to be generally *non-local* in Λ , i.e. the flow of the vertex at a given step of the renormalization depends on the values of the vertex at former steps. This is certainly not a pleasant but (as far as we can see) necessary property of the KWP procedure if we want to keep more than just the purely logarithmic contributions.

We then apply the one–loop KWP renormalization group to the Hubbard model. One further approximation we make is to consider the effective interaction as a function only of the projection of the momenta to the square Fermi surface (marginal interactions) while the radial dependence and dynamics are neglected because they are irrelevant

with respect to the Fermi–liquid scaling.³⁰ We neglect also the renormalization of the self–energy. If we take only marginal interactions into account this is justified at the one–loop level because the renormalization of the weight and of the lifetime of the electrons receives a nonzero contribution only at the two–loop level. We thus renormalize only the interaction $U(\theta_1, \theta_2, \theta_3)$, a function of three angular variables corresponding to the angular parts of the three external momenta, the fourth being determined by momentum conservation. We allow the θ –variables to be anywhere on the almost square Fermi surface and not only in the configurations that give perfect nesting or zero center–of–the–mass momentum: these two classes of the configurations would correspond only to the processes with the leading logarithmic renormalization in the p–h and p–p channels, respectively. As will become clear later, taking all three θ –variables without constraints is the essential point of the calculation because the coupling between p–p and p–h channels is appears mostly through interactions that have other than just leading–logarithmic flow. This is a special feature of the square or almost square Fermi surface and can be handled only by the non–local (outer–shell) contributions to the flow, using the Polchinski equation.

The first aim of our calculation is to find the temperature at which the system flows towards strong coupling. We associate this temperature with a mean–field like critical temperature and call it T_c^{RG} . A typical mean–field theory then is regularized for $T < T_c$ by adding counterterms that contain fermions bilinearly coupled to some order parameter. In our theory the order parameter is not known a priory: it is determined by the manner in which the *function* $U(\theta_1, \theta_2, \theta_3)$ diverges at $T = T_c^{RG}$. We perform a detailed analysis of the behavior of the angle–resolved correlation functions for antiferromagnetism and superconductivity and obtain the type and the symmetry of the order parameter determining the dominant correlations near the T_c^{RG} . The final result is the analogue of a mean–field phase diagram of the Hubbard model. We are considering a two–dimensional system where one should be careful about the interpretation of T_c : in the case of magnetism, this indicates the onset of well–defined finite–range correlations. For weak interactions, this is typically a very well–defined crossover.³⁴ In the case of pairing T_c^{RG} can be identified with the onset of quasi–long–range order. However, in real systems like copper oxides even a weak inter–plane two–particle hopping (particle–hole–pair hopping for antiferromagnetism or Josephson tunneling for superconductivity) stabilizes a 3D long–range order.

In section II we begin by the formulation of the many fermion system on a lattice in terms of functional integrals. We introduce the concept of the effective action and show how it can be formally calculated using the partial trace technique. We than derive the Kadanoff–Wilson–Polchinski exact renormalization group as one possible strategy for calculating the effective action in terms of the renormalization group flow of all vertices. Truncating the effective action at the level of sixth order vertices we obtain the one loop renormalization group equations for the effective interaction and for the selfenergy. In section III we apply the zero–temperature one–loop renormalization group to the Hubbard model on a square lattice. We derive the flow equations for the effective interaction function and for the angle–resolved correlation functions of superconducting and antiferromagnetic type. After discretization of the angle θ on the Fermi surface we integrate numerically the flow and present the resulting phase diagram. In section IV we introduce finite temperature explicitly in the renormalization group equations. We then calculate the fixed point values of the correlation functions at temperatures near the instability. The conclusions are given in section V.

II. FORMULATION OF THE RENORMALIZATION GROUP FOR A MANY-FERMION PROBLEM ON A LATTICE

The simplest model for interacting fermions on a two-dimensional square lattice is the Hubbard Hamiltonian

$$H = -t \sum_{\langle i,j \rangle, \sigma} (a_{i,\sigma}^\dagger a_{j,\sigma} + a_{j,\sigma}^\dagger a_{i,\sigma}) + \frac{U_0}{2} \sum_i n_i n_i - \mu \sum_i n_i \quad (2.1)$$

where $a_{i,\sigma}(a_{i,\sigma}^\dagger)$ is the creation (annihilation) operator of an electron at the site i with spin σ , t is the inter-site transfer integral, μ is the chemical potential, and U_0 is the on-site Coulomb repulsion. After Fourier transform, the Hamiltonian writes

$$H = \sum_{\sigma \mathbf{k}} \xi_{\mathbf{k}} a_{\sigma \mathbf{k}}^\dagger a_{\sigma \mathbf{k}} + \frac{1}{2} \sum_{\sigma} \sum_{\mathbf{k}_1, \mathbf{k}_2, \mathbf{k}_3} U_0 a_{-\sigma, \mathbf{k}_1 + \mathbf{k}_2 - \mathbf{k}_3}^\dagger a_{-\sigma \mathbf{k}_2} a_{\sigma \mathbf{k}_3}^\dagger a_{\sigma \mathbf{k}_1} , \quad (2.2)$$

where

$$\xi_{\mathbf{k}} = -2t(\cos k_x + \cos k_y) - \mu \quad (2.3)$$

and the momenta are within the first Brillouin zone. In this section we want to derive the renormalization group for a more general problem. For that purpose we allow $\xi_{\mathbf{k}}$ to have a general dependence on \mathbf{k} . Furthermore, we suppose that the interaction can be nonlocal and dynamical, that is, we suppose that it depends on energies and momenta of the interacting particles.

The statistical mechanics of such general model is given by the partition function³⁰

$$Z = \int \mathcal{D}\bar{\Psi} \mathcal{D}\Psi e^{S\{\Psi\}} \quad (2.4)$$

where the functional integration is over Grassmann variables $\bar{\Psi}(\Psi)$ for all electrons in the Brillouin zone. The action S is given by

$$\begin{aligned} S\{\Psi\} = S_0\{\Psi\} + S_I\{\Psi\} = & T \sum_{\omega_n} \sum_{\sigma \mathbf{k}} \bar{\Psi}_{\sigma K}(i\omega_n - \xi_{\mathbf{k}}) \Psi_{\sigma K} + \\ & + \frac{1}{2} \sum_{\sigma \sigma'} T^3 \sum_{\omega_{n_1}, \omega_{n_2}, \omega_{n_3}} \sum_{\mathbf{k}_1, \mathbf{k}_2, \mathbf{k}_3} U_0(K_1, K_2, K_3) \bar{\Psi}_{\sigma K_3} \bar{\Psi}_{\sigma' K_4} \Psi_{\sigma' K_2} \Psi_{\sigma K_1} . \end{aligned} \quad (2.5)$$

The variables $\bar{\Psi}(\Psi)$ are labeled by the energy-momentum vector $K = (\omega_n, \mathbf{k})$. $\xi_{\mathbf{k}}$ is the bare spectrum measured from the Fermi level:

$$\xi_{\mathbf{k}} = \epsilon_{\mathbf{k}} - \mu ,$$

where $\epsilon_{\mathbf{k}}$ is the band dispersion and μ the chemical potential. The energies and momenta are conserved so that $K_4(K_1, K_2, K_3) = (\omega_{n_1} + \omega_{n_2} - \omega_{n_3}, \mathbf{k}_1 + \mathbf{k}_2 - \mathbf{k}_3)$. $U_0(K_1, K_2, K_3)$ is the most general spin independent interaction, a function of the frequencies and momenta. The derivation of the action (2.5) for a general model is equivalent to the derivation for the Hubbard model^{33,35}, provided that we put $U_0(K_1, K_2, K_3)$ instead of the constant U_0 and keep $\xi_{\mathbf{k}}$ general.

We want to derive the low energy effective action (LEEA) for this model. The low energy modes are the electronic degrees of freedom close to the Fermi surface. We will use this criterion and use the energy variable $\xi_{\mathbf{k}}^0$ to discriminate fast (high-energy) modes $\Psi_>$ from the slow (low-energy) ones $\Psi_<$. Let's choose some arbitrary nonzero high energy cutoff Λ defining a shell of wavevectors around the Fermi surface. The electronic variables can then be written

$$\Psi_{\sigma,K} = \theta(|\xi_{\mathbf{k}}| - \Lambda)\Psi_{>,\sigma,K} + \theta(\Lambda - |\xi_{\mathbf{k}}|)\Psi_{<,\sigma,K}. \quad (2.6)$$

The slow modes are inside the shell $\pm\Lambda$ while the fast ones are outside, with $|\xi_{\mathbf{k}}|$ going up to the physical cutoff Λ_0 taken to be equal to the bandwidth so that we are sure that the whole Brillouin zone is taken into account. Note that the cutoff is imposed only on momentum space, while the Matsubara frequencies remain unlimited. The LEEA $S_{\Lambda}\{\Psi_<\}$ is an action containing only slow modes and gives the same partition function as S eq.(2.5), or formally

$$Z = \int \mathcal{D}\bar{\Psi}_< \mathcal{D}\Psi_< e^{S_{\Lambda}\{\Psi_<\}}, \quad (2.7)$$

This means that $S_{\Lambda}\{\Psi_<\}$ is calculated by taking the *partial trace* over only fast modes in eq.(2.4):

$$S_{\Lambda}\{\Psi_<\} = \ln \int \mathcal{D}\bar{\Psi}_> \mathcal{D}\Psi_> e^{S\{\Psi_<, \Psi_>\}} \quad (2.8)$$

The LEEA contains a new effective kinetic part $S_{0\Lambda}$ with a finite selfenergy term and a new interaction $S_{I\Lambda}$. We have *chosen* that the Fermi surface for the bare electrons plays the role of the zero energy manifold. This still does not mean that we make the approximation of a Fermi surface unrenormalized by interactions: even if the Fermi surface of the LEEA is different from the bare one we are still allowed to use $\xi_{\mathbf{k}}^0$ for the bookkeeping of our mode elimination.

If we consider the slow modes as parameters, expression (2.8) can be evaluated, at least formally, using the linked cluster theorem.³³ The result is composed of three terms:

$$S_{\Lambda}\{\Psi_<\} = S\{\Psi_<\} + \Omega_> + \delta S\{\Psi_<\} \quad (2.9)$$

Only the interaction part S_I of the action S can mix slow and fast modes:

$$S_I = S_I\{\Psi_<\} + S_I\{\Psi_>\} + S_I\{\Psi_<, \Psi_>\} \quad (2.10)$$

while S_0 is diagonal and can contain only one kind of modes in the same term:

$$S_0 = S_0\{\Psi_<\} + S_0\{\Psi_>\}. \quad (2.11)$$

The first term in the equation (2.9) is then only a constant from the point of view of the fast electrons and is equal to $S_0\{\Psi_<\} + S_I\{\Psi_<\}$. $\Omega_>$ is the grand potential (times β) of the fast electrons as if they were decoupled from the slow ones:

$$\Omega_> = - \sum_{\mathbf{k}>} \ln(1 + e^{-\beta\xi_{\mathbf{k}}}) + \sum_{\mathbf{k}>} (\text{all connected clusters with } S_I\{\Psi_>\}). \quad (2.12)$$

This term gives only a shift of the total free energy of the system.

The term $\delta S\{\Psi_<\}$ in eq.(2.9) is the most interesting one. It brings the corrections due to the scattering processes of the slow modes on the fast ones into the LEEA and is given by the sum of all connected graphs composed of

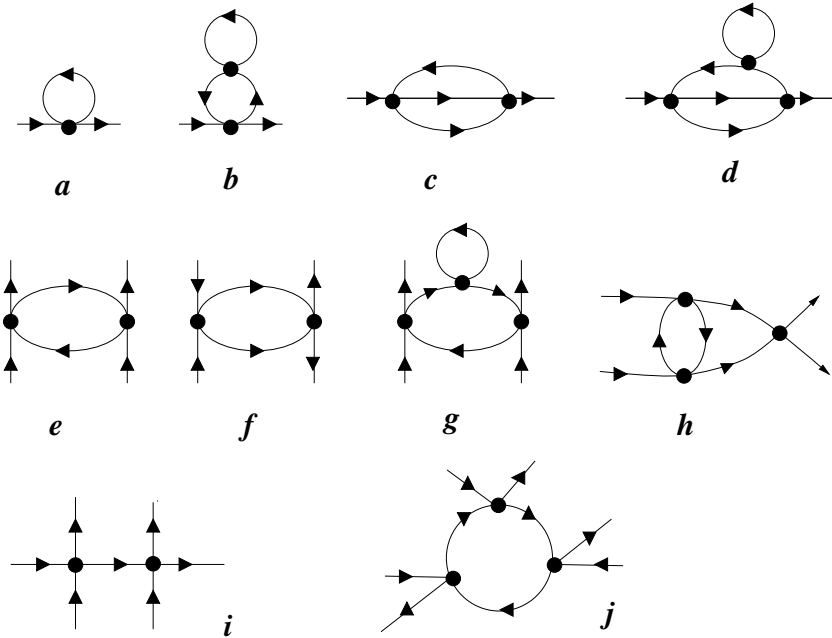


FIG. 1. A few lowest order cumulants for $\delta S\{\Psi_<\}$. All internal lines are integrated only over the fast ($>$) modes.

$S_I\{\Psi_>\} + S_I\{\Psi_<, \Psi_>\}$. If we draw the slow modes as external legs, the diagrams for $\delta S\{\Psi_<\}$ are the clusters with at least two legs. A few low order diagrams for $\delta S\{\Psi_<\}$ are given in fig. 1. The terms with two external legs, labeled by *a*, *b*, *c*, and *d* in figure 1 are the selfenergy terms, renormalizing S_0 . The terms with four legs: *e*, *f*, *g* and *h* renormalize the quartic interaction term S_I . The terms with six (*i* and *j*) and more legs are new! They are *created* by the mode elimination procedure.

Of physical interest is the LEEA for the electrons in the very vicinity of the Fermi surface ($\Lambda \ll E_F$). Even if the coupling is small some of the loop diagrams will attain at low temperature ($T < \Lambda$) large values depending of the form of the Fermi surface. For example, if the Fermi surface is not close to van Hove singularities the particle-particle (p-p) diagram (*f* in fig. 1) for the four-point vertex with zero center of the mass momentum always has a logarithmic dependence like $\log(\Lambda_0/\Lambda)$, where Λ_0 is the initial cutoff equal to the bandwidth. If the Fermi surface is nested the particle-hole (p-h) diagram (*e* in fig. 1) at $2\mathbf{k}_F$ behaves in the same way. In the Hubbard model close to half-filling the van Hove singularities make both loops squares of logarithms. The perturbative calculation of the expansion (2.12) for small U_0 is thus not straightforward: at least some of sets of diagrams, containing *both* p-p and p-h subdiagrams, have to be summed entirely. The lowest order diagram of that kind is the one denoted by *h* in fig. 1. On the other hand the truncation of the LEEA at fourth order is in general allowed for weak coupling. However the direct summation of cumulants for $\delta S\{\Psi_<\}$ (like T-matrix or RPA summation) can be performed in a useful and controlled way only for a limited number of physical problems, that is when some subsets of diagrams are dominant. The direct parquet summation for a general Fermi surface in more than one dimensions is probably very hard. It has been done only for the case of perfectly nested (flat) Fermi surface^{19,20}.

The problem is even more difficult if the coupling is not small. Then the criteria of most important sets of diagrams are not clear any more and even the truncation of LEEA at quartic or sextic term in $\Psi_<$ is not justified any more.

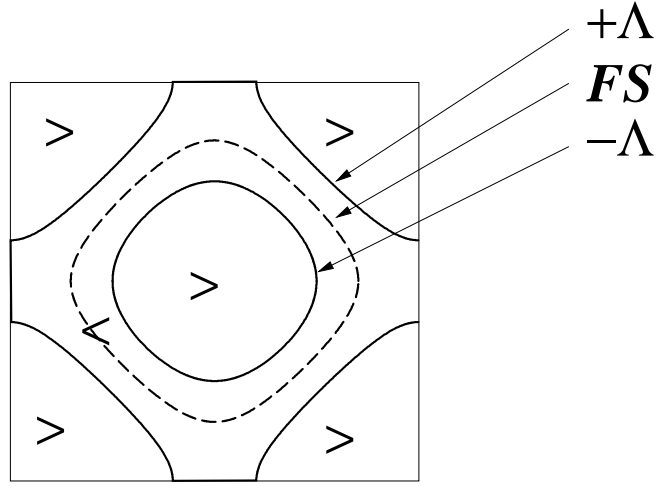


FIG. 2. The division of the Brillouin zone into the outer-shell ($>$), the on-shell (l), and the slow ($<$) modes.

A. Kadanoff–Wilson–Polchinski renormalization group: Exact formulation

A tractable way to construct the *exact* LEEA is to use the Kadanoff–Wilson–Polchinski renormalization group. Let us call the initial cutoff (the bandwidth) Λ_0 and parameterize Λ by the renormalization parameter l so that $\Lambda = \Lambda_0 \exp(-l)$. The idea of the renormalization group is to consider the transformation $S \equiv S_{\Lambda_0} \rightarrow S'_{\Lambda_0 \exp(-l)}$ as an infinite set of infinitesimal mode eliminations

$$S_{\Lambda_0} \rightarrow S_{\Lambda_0 \exp(-dl)}^{(1)} \rightarrow S_{\Lambda_0 \exp(-2dl)}^{(2)} \rightarrow \dots \rightarrow S'_{\Lambda_0 \exp(-l)} \quad (2.13)$$

At each step we eliminate Λdl of modes at a distance Λ from both sides of the Fermi surface. We will see that the mode elimination of an infinitesimal shell of degrees of freedom is much simpler than the one-step procedure discussed in the previous section.

From now on we will call the LEEA simply the effective action because in the process of successive mode elimination (2.13) Λ can have any value between Λ_0 and zero. Indeed, it is of physical interest to follow the flow of the effective action S_Λ as Λ decreases.

We now concentrate to one single step $l \rightarrow l + dl$ of the mode elimination. We call *outer shell* modes the modes already eliminated by the previous steps (the fast ($>$) modes). The modes inside the shell $[\Lambda_0 \exp(-l) - \Lambda_0 \exp(-l - dl)]$ are the ones to integrate out. We call them *on-shell* modes and denote them by (l). Figure 2 shows the division of the Brillouin zone into three types of modes ($>$, l , and $<$) for the case of the non-half-filled Hubbard model.

If l is not the very first step, the effective action S_Λ contains couplings of all orders. Schematically it reads

$$S_\Lambda = S_{0\Lambda} + S_{I\Lambda} = \Gamma_2^{(l)} \bar{\Psi} \Psi + \Gamma_4^{(l)} \bar{\Psi} \bar{\Psi} \Psi \Psi + \Gamma_6^{(l)} \bar{\Psi} \bar{\Psi} \bar{\Psi} \Psi \Psi \Psi + \dots \quad (2.14)$$

The summation over all frequencies, momenta, and spins is assumed. The two point vertex Γ_2 defines Wick's theorem at step l . In particular the propagator of the “bare electrons” Γ_2^{-1} changes as we proceed with the renormalization.

The construction of the effective action one step further (at $l + dl$) is of the same form as the equation (2.9), with the difference that now the on-shell modes play the role of the fast modes. As we are interested only in the renormalization of vertices, we can skip the constant Ω and we get the recursion relation:

$$S_{\Lambda(l+dl)} = S_{\Lambda(l)} + \delta S(l) . \quad (2.15)$$

The contribution $\delta S(l)$ is due to the elimination of l modes. It is given by the sum of all cumulants made of $S_{I\Lambda}\{\Psi_l\}$ and $S_{I\Lambda}\{\Psi_l, \Psi_<\}$ with two or more legs but now with all internal momenta constrained to be on-shell. Now we use the fact that $d\Lambda$ is infinitesimal: In the expression for $\delta S(l)$ only the terms linear in dl will survive, to make the recursion (2.15) a differential equation for $S_{\Lambda(l)}$. Generally the cumulants with m internal lines are proportional to $d\Lambda^m$ because every internal line is constraint to the shell. In principle only diagrams with one internal line are proportional to dl . If we group the terms with equal number of legs, we obtain the flow equation for vertices $\Gamma_n^{(l)}$, known as Polchinski equation for the vertices.^{31,32} Only two types of diagrams with one internal line are possible: tree diagrams and loop diagrams. The Polchinski equation for the vertices is shown on fig.3. Its symbolical form for a two-point vertex ($2n = 2$) is

$$\frac{\partial}{\partial \Lambda_l} \Gamma_2^{(l)}(K) = -T \sum_{\omega_n} \int_{d\Lambda} d^2 k' \Gamma_4^{(l)}(K', K, K', K) G_l(K') . \quad (2.16)$$

This means that only the loop term renormalizes the selfenergy (see figure 3). Both loop and tree terms are present in the Polchinski equation for the higher order vertices:

$$\begin{aligned} \frac{\partial}{\partial \Lambda_l} \Gamma_{2n}^{(l)}(K_1, \dots, K_n, K_{n+1}, \dots, K_{2n}) &= \sum_{I_1, I_2} T \sum_{\omega_n} \int_{d\Lambda} d^2 k \Gamma_{2n_1}^{(l)}(-K, I_1) G_l(K) \Gamma_{2n_2}^{(l)}(K, I_2) - \\ &- T \sum_{\omega_n} \int_{d\Lambda} d^2 k \Gamma_{2(n+1)}^{(l)}(K, K_1, \dots, K_n, K, K_{n+1}, \dots, K_{2n}) G_l(K) . \end{aligned} \quad (2.17)$$

The two-point vertex defines the one-particle propagator G_l at each step of the renormalization:

$$G_l(K) = (\Gamma_2^{(l)}(K))^{-1} \quad (2.18)$$

We use this *renormalized* propagator to construct the Wick theorem. We name $\Gamma_{2n}^{(l)}(K_1, \dots, K_n, K_{n+1}, \dots, K_{2n})$ the vertex with $2n$ external legs at the step l of the renormalization, with legs $\{K_1, \dots, K_n\}$ coming in and $\{K_{n+1}, \dots, K_{2n}\}$ coming out. Symbols I_1 and I_2 in equation (2.17) are disjoint subsets ($I_1 \cap I_2 = \emptyset$) of the energy-momenta such that $I_1 \cup I_2 = \{K_1, \dots, K_{2n}\}$. The sum runs over all such sets. We have skipped spin indices for simplicity.

We see that the Polchinski flow equation is a functional equation because all vertices are renormalized as *functions* of momenta and frequencies. It gives the exact renormalization group flow of the model. The careful reader will perhaps hesitate at this point: some of the loop diagrams with *two* internal lines as for example the p-p diagrams are also proportional to just dl if we put the total momentum and energy to zero. The same “anomaly” happens if the nesting is perfect for some p-h diagrams. In the usual renormalization group calculations only these contributions are taken into account³⁰ because they give the dominant logarithmic part of the renormalization group flow. Then one

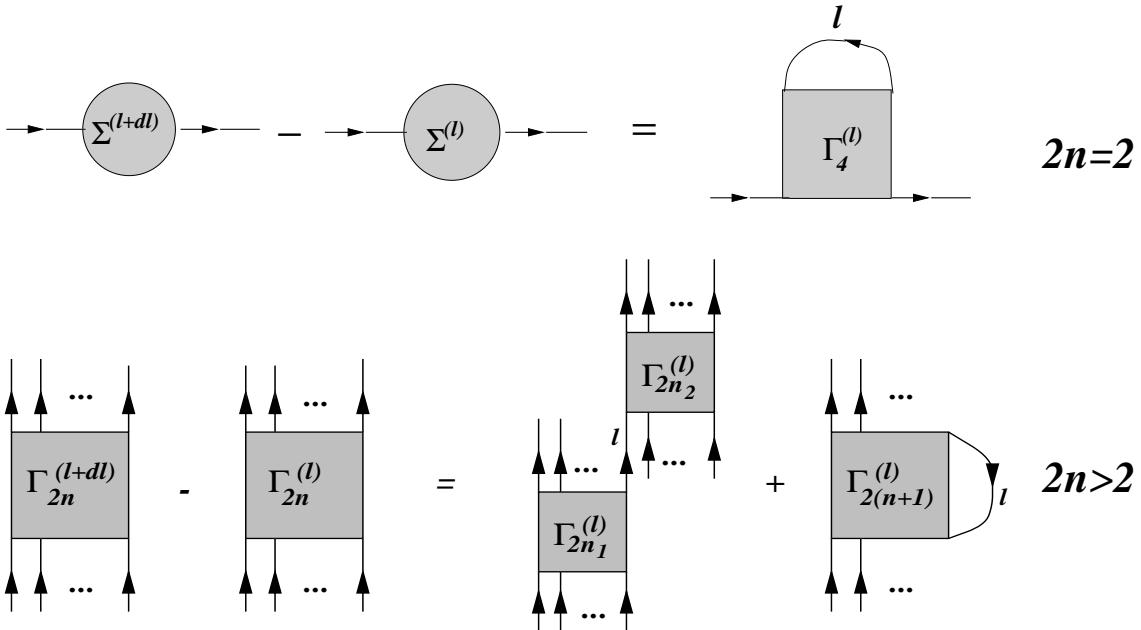


FIG. 3. Polchinski equation for the vertices with $n = 2$ and $n > 2$ legs.

misses all non-logarithmic or ‘‘almost logarithmic’’ physics. This is not a problem in one dimension, for example. But if we are in two or more dimensions and especially if the nesting is good but not perfect, it is better to consider the exactly logarithmic configurations of energy-momentum as exceptions. If we formulate the flow equations correctly for the general case, the exact logarithmic terms will also appear, as we will see in the next subsection.

In principle vertices of all orders are created with increasing powers of the initial coupling U_0 : It is easy to see that the vertex Γ_{2n} , ($n > 2$), is created by the tree term of the Polchinski equation with power $(n-1)$ of the bare coupling. This means that the truncation of the expansion (2.14) is equivalent to weak-coupling perturbation theory.

B. Truncation of the Polchinski equation: one-loop renormalization group

The one-loop renormalization for the vertex Γ_4 (or for the effective interaction U_l) is the perturbative procedure to truncate the flow equations at order U^2 . All terms of order higher than six in the expansion (2.14) are created with a power higher than 2 of the interaction by the tree term of the Polchinski equation. Thus putting $\Gamma_8 = \Gamma_{10} = \dots = 0$, we generate the one-loop renormalization group. The only contribution to the vertex Γ_6 is then the tree term, made of two Γ_4 terms connected by one line (see figure 4(a)). The line denoted with l has in principle to be taken dressed by the selfenergy at the step l defined as

$$\Sigma_l \equiv \Gamma_2^{(l)} - \Gamma_2^0 = \Gamma_2^{(l)} - i\omega_n + \xi_{\mathbf{k}}^0. \quad (2.19)$$

We assume that the selfenergy remains diagonal upon renormalization. This is consistent with the weak-coupling treatment because off-diagonal terms would imply the existence of some form of long-range order, which is out of the reach of the present calculation. All we can possibly expect from our calculation is a divergence of some effective interaction signalling the *onset* of long-range order.

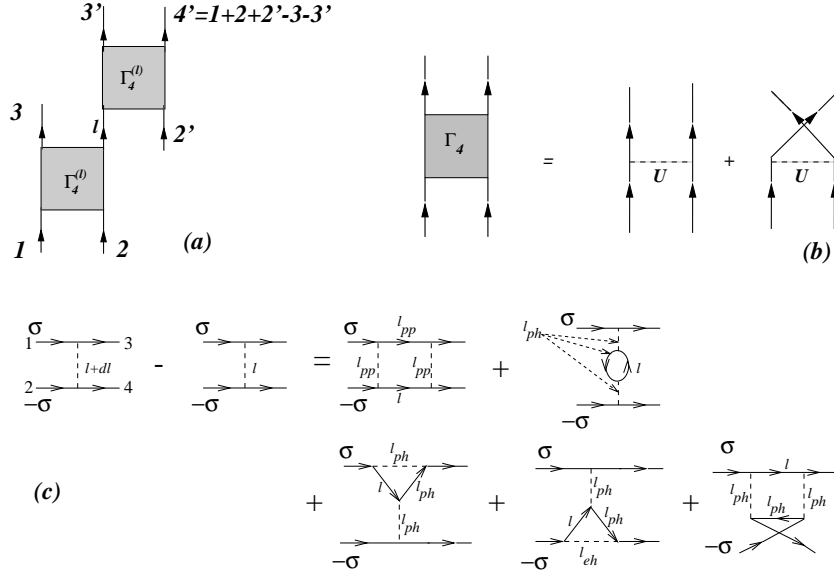


FIG. 4. (a) The six-point vertex for one-loop renormalization group. (b) Relation between the vertex Γ_4 and the interaction U . (c) Recursion for the one-loop renormalization of the interaction U .

We now go back to the formulation in terms of the interaction as defined by eq.(2.5) and illustrated in fig.4(b). We will skip the spin indices where they are not necessary. The differential flow of the six point function Γ_6 at step l is according to the fig.4(a) given by

$$d\Gamma_6^{(l)}(K_1, K_2, K_3, K'_2, K'_3) = T \sum_{\omega_n} \int_{d\Lambda} d^2k \delta(\mathbf{k} - \mathbf{k}_1 - \mathbf{k}_2 + \mathbf{k}_3) \delta_{\omega_n - \omega_{n1} - \omega_{n2} + \omega_{n3}} \times G_l(K) U_l(K_1, K_2, K_3) U_l(K, K'_2, K'_3). \quad (2.20)$$

The phase space integral is over the shell of thickness $d\Lambda$ corresponding to step l , and $G_l(K)$ is the renormalized Green function at the same step. Physically this is the propagator of an on-shell electron renormalized by the scattering on the fast electrons. $U_l(K_1, K_2, K_3)$ is the effective interaction at step l . The vertex Γ_6 at some step l is the integral of eq.(2.20) over all steps between $\Lambda = \Lambda_0$ and Λ_l , that is over all fast degrees of freedom. On the other hand, there is no loop integration in this term: the Dirac function in equation (2.20) reduces the integral $\int_{d\Lambda} d^2k$ to a single point $\mathbf{k} = \mathbf{k}_1 + \mathbf{k}_2 - \mathbf{k}_3 (= \mathbf{k}_{3'} + \mathbf{k}_{4'} - \mathbf{k}_{2'})$. To get Γ_6 we can thus skip the integration over dl and take just care of momentum conservation. The effective action at the step l then reads

$$S_l = \sum_{\omega_n, \mathbf{k}} \bar{\Psi}_{K, \sigma}(i\omega_n - \xi_{\mathbf{k}} + \Sigma_l(K)) \Psi_{K, \sigma} \Theta(\Lambda(l) - |\xi_{\mathbf{k}}|) + \frac{1}{2} T^3 \sum_{\sigma \sigma'} \sum_{1,2,3} U_l(K_1, K_2, K_3) \Theta_{\mathbf{k}_1, \mathbf{k}_2, \mathbf{k}_3, \mathbf{k}_4}^{(\Lambda(l))} \bar{\Psi}_{\sigma K_3} \bar{\Psi}_{\sigma' K_4} \Psi_{\sigma' K_2} \Psi_{\sigma K_1} + T^5 \sum_{\sigma, \sigma', \sigma''} \sum_{1,2,3,2',3'} [\Theta_{\mathbf{k}_1, \mathbf{k}_2, \mathbf{k}_3, \mathbf{k}_2', \mathbf{k}_3', \mathbf{k}_4}^{(\Lambda(l))} \Theta(|\xi_{\mathbf{k}}| - \Lambda(l)) \times G_{l'}(K) U_{l'}(K_1, K_2, K_3) U_{l'}(K, K'_2, K'_3) \bar{\Psi}_{\sigma K_3} \bar{\Psi}_{\sigma' K_3'} \bar{\Psi}_{\sigma'' K_4'} \Psi_{\sigma'' K_2'} \Psi_{\sigma' K_2} \Psi_{\sigma K_1}], \quad (2.21)$$

where $l' = \ln \Lambda_0 / |\xi_{\mathbf{k}}|$ (i. e. $\xi_{\mathbf{k}} = \Lambda(l')$) is the scale fixed by external momenta, $K = K_1 + K_2 - K_3$ and the energy-momentum $4' = 1 + 2 + 2' - 3 - 3'$. The summations over $1,2,3,\dots$ run over corresponding Matsubara frequencies and momenta. The term of the sixth order contains the interactions and Green functions from former steps $l' < l$ of

the mode elimination since only fast degrees of freedom contribute to Γ_6^l so that $l' \leq l$. This constraint is imposed to the sextic term of action (2.21) by $\Theta(|\xi_{\mathbf{k}}| - \Lambda(l))$. The functions $\Theta_{\mathbf{k}_1, \mathbf{k}_2, \mathbf{k}_3, \mathbf{k}_4}^{(\Lambda)}$ and $\Theta_{\mathbf{k}_1, \mathbf{k}_2, \mathbf{k}_3, \mathbf{k}'_2, \mathbf{k}'_3, \mathbf{k}'_4}^{(\Lambda)}$ constrain the momenta in arguments to be slow modes (inside a shell of thickness $\pm\Lambda$ around the Fermi surface). This simply means that the fields described by the effective action at cutoff $\Lambda(l)$ are inside the cutoff range.

If the initial interaction U_0 is spin independent, the renormalized interaction U_l will remain spin independent as well. It is thus not necessary to worry about spin indices and all two-particle interactions are given only by *one* function $U_l(1, 2, 3)$. The detailed justification for that is given in the appendix A. The differential flow of $U_l(1, 2, 3)$ is readily obtained applying the loop term of the Polchinski equation (the second term in equation (2.17) and in figure 3(b)) to the six-leg part of the effective action (2.21). At first sight, two kinds of diagrams are created: one-particle reducible (1PR) and one-particle irreducible (1PI) ones. We will show that only 1PI diagrams contribute to the renormalization of the effective interaction : We can try to construct the 1PR diagram by contracting legs 2' and 4' in figure 4(a). This immediately implies that the internal line denoted with l and the leg 3' carry the same momentum. This momentum corresponds to some fast mode since line l is already integrated out. The conclusion is that the resulting four-point 1PR vertex can not be a vertex of the effective action (2.21) since this action contains only slow modes. Consequently, only 1PI diagrams renormalize the effective interaction between slow electrons. The resulting diagrams are all topologically different two-particle loops as shown on figure 4(c). The first diagram is a p-p diagram and the others are p-h diagrams. Let us illustrate how we obtain the first diagram in fig. 4(c). The procedure is shown on fig. 5. The diagram represents the p-p contribution to the effective interaction $U_l(1, 2, 3)$ due to the elimination of the infinitesimal shell at step l . We take the six-leg diagram with the configuration of external momenta shown in the figure and with legs K being on-shell. Their contraction (dashed line) is done precisely at step l . The contraction K' was done at a previous step l_{pp} fixed by momenta K , K_1 , and K_2 (see equation (2.20)). $K_1 + K_2 = Q_{pp} \equiv (\omega_{pp}, \mathbf{q}_{pp})$ is the total energy-momentum in the p-p process. The scale l_{pp} is then given by

$$l_{pp} = -\ln \frac{\xi_{\mathbf{k}} - \mathbf{q}_{pp}}{\Lambda_0}. \quad (2.22)$$

Similar constructions give all other (p-h) diagrams. One has to take care of both direct and exchange interactions (fig. 4(b)) to get four different graphs. The interactions and one-particle propagators are to be taken at the scale $l_{ph} \leq l$. This scale is determined by the momentum transfer \mathbf{q}_{ph} as

$$l_{ph} = -\ln \frac{\xi_{\mathbf{k}} + \mathbf{q}_{ph}}{\Lambda_0}. \quad (2.23)$$

In second, third, and fourth diagram in fig. 4(c) the energy-momentum transfer is $Q_{ph} = K_1 - K_3$, while in the last diagram $Q_{ph} = K_1 - K_4$.

We see that even though the Polchinski equation appears as local in l , the flow at step l depends on the Green functions and interactions at the former steps $l_{pp}, l_{ph} \leq l$. The reason for that is the dependence of the six point function on two-particle interaction and on one-particle propagator at all former steps.

In fig. 4(c) the internal lines labeled with l are to be integrated over two infinitesimal shells of the width $d\Lambda$ at $\xi_0 = \pm\Lambda_l$. For this purpose we pass from the Cartesian measure $dk_x dk_y$ to the measure

$$\int_{\xi}^{\xi+d\Lambda} d\xi' \oint \frac{ds}{v(s, \xi')}, \quad (2.24)$$

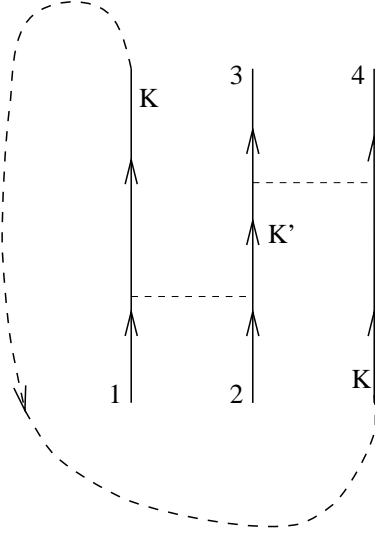


FIG. 5. Construction of the p-p diagram from the six-leg vertex.

where s are lines (or surfaces in $D > 2$) of constant energy $\xi(\mathbf{k})$ and $v(s, \xi')$ is the group velocity as defined by $\partial\xi(\mathbf{k})/\partial k_\perp$ (k_\perp is the component of the momentum perpendicular to the equal-energy lines). We will use measure (2.24) in what follows, where we write the analytic expression for the flow of function $U_l(1, 2, 3)$.

From the diagrams in fig.4(c) one obtains the following expression

$$\begin{aligned} \frac{\partial U_l}{\partial l} &= \beta(l, \{U\}) \\ &= \beta_{pp}\{U, U\} + 2\beta_{ph}\{U, U\} - \beta_{ph}\{U, XU\} - \beta_{ph}\{XU, U\} - X\beta_{ph}\{XU, XU\}. \end{aligned} \quad (2.25)$$

β is a four point object and a bilinear functional of $U_{l'}$, ($l' \leq l$). The operator X is the exchange operator acting on a four-point function: $XF(1, 2, 3, 4) \equiv F(2, 1, 3, 4)$. β_{pp} and β_{ph} are the p-p and p-h parts of the β function given by

$$\beta_{pp}\{U, U\} = (\Xi\{U, U\} + \Xi\{XU, XU\}) \quad (2.26)$$

$$\beta_{ph}\{U_1, U_2\} = (\Pi\{U_1, U_2\} + \mathcal{T}\Pi\{U_1, U_2\}). \quad (2.27)$$

\mathcal{T} is the time inversion operator acting on a four point function: $\mathcal{T}F(1, 2, 3, 4) \equiv F(3, 4, 1, 2)$. The functions Ξ and Π correspond to the on-shell integrals of the p-p and p-h bubbles:

$$\begin{aligned} \Xi\{U, U\}(K_1, K_2, K_3, K_4) &= \frac{-\Lambda_l}{(2\pi)^2} \sum_{\nu=+,-} \int \frac{ds_\nu}{v_\nu} \Theta(|\xi_{\mathbf{k}_\nu - \mathbf{q}_{pp}}| - \Lambda_l) T \sum_{\omega_n} G_l(K_{(\nu)}) G_{l_{pp}}(-K_{(\nu)} + Q_{pp}) \\ &\times U_{l_{pp}}(K_1, K_2, K_{(\nu)}) U_{l_{pp}}(K_3, K_4, K_{(\nu)}), \end{aligned} \quad (2.28)$$

$$\begin{aligned} \Pi\{U_1, U_2\}(K_1, K_2, K_3, K_4) &= \frac{-\Lambda_l}{(2\pi)^2} \sum_{\nu=+,-} \int \frac{ds_\nu}{v_\nu} \Theta(|\xi_{\mathbf{k}_\nu + \mathbf{q}_{ph}}| - \Lambda_l) T \sum_{\omega_n} G_l(K_{(\nu)}) G_{l_{ph}}(K_{(\nu)} - Q_{ph}) \\ &\times U_{1,l_{ph}}(K_1, K_{(\nu)}, K_3) U_{2,l_{ph}}(K_4, K_{(\nu)}, K_2). \end{aligned} \quad (2.29)$$

U_1 et U_2 can be U or XU as required by eq.(2.25). The summation over index $\nu = +, -$ is over two shells at $\xi_0 = \pm \Lambda_l$; the velocities are $v_\nu = v(s_\nu, \xi = \nu \Lambda)$ and K_ν symbolizes $(\mathbf{k}_\nu, \omega_n)$. The quantity

$$Q_{pp} = (\omega_{n,pp}, \mathbf{q}_{pp}) = K_1 + K_2$$

is the total energy-momentum and

$$Q_{ph} = (\omega_{n,ph}, \mathbf{q}_{ph}) = K_1 - K_3,$$

is the energy-momentum transfer between the currents (1,3) and (2,4) where 1,2,3 and 4 are the external variables of Ξ and Π . The scales l_{pp} and l_{ph} are defined by expressions (2.22) and (2.23). As already discussed, l_{pp} and l_{ph} depend on the integration variable \mathbf{k}_ν and on the configuration of the external energies-momenta. Let's call the external legs of the total β function (2.25) $\tilde{1}, \tilde{2}, \tilde{3}$ and $\tilde{4}$. Note that the operator X exchanges the external legs $\tilde{1}$ and $\tilde{2}$ in the last term of this expression. This means that the energy-momentum transfer in this term is $Q_{ph} = K_{\tilde{1}} - K_{\tilde{4}}$ and not $K_{\tilde{1}} - K_{\tilde{3}}$ as in the first three e-h terms. In the standard language (see for example ref. 30) the p-h terms with transfer $1 - 3$ are called zero-sound (ZS) terms, and the terms with transfer $1 - 4$ are ZS'.

Let us explain briefly how we obtained the flow equation (2.25). The first term is simply the p-p loop with U interaction. The remaining terms are different versions of the p-h loops, corresponding respectively to the p-h diagrams in the figure 4(c). They can all be seen as a single loop β_{ph} (with the topology of the second diagram in fig.4(c)), given by (2.27) and (2.29) by performing appropriately the operation X . The third and the fourth graph can be drawn as the second one by one exchange: In the third term we replace the upper interaction line U by XU and in the fourth the lower one. After this manipulation both diagrams look like the second diagram. The last graph is more complicated: one has to perform X upon both interactions and upon the whole graph to see it as β_{ph} . The factor 2 before the second term is due to spin summation in the loop. All other diagrams have fixed spin.

The flow of the effective action (2.21) is still not completely determined because we do not know how the self-energy $\Sigma_l(K)$ is renormalized. The differential flow for $\Sigma_l(K)$ is readily found from the Polchinski equation for the two-point function (2.16) shown graphically in fig.3. In the language of the effective interaction $U_l(1, 2, 3)$ this gives Hartree and Fock like contributions shown in the fig.4(c). We get the renormalization equation

$$\frac{\partial \Sigma}{\partial l(K_1)} = \alpha_{\text{Hartree}}\{U_l\}(K_1) + \alpha_{\text{Fock}}\{U_l\}(K_1) + \alpha_\mu^{\text{hom.}}(l). \quad (2.30)$$

The first term is the Hartree term

$$\alpha_{\text{Hartree}}\{U_l\}(K_1) = \frac{\Lambda}{(2\pi)^2} \sum_{\nu=+,-} \int \frac{ds_\nu}{v_\nu} T \sum_{\omega_n} G_l(K_\nu) \frac{1}{2} (3 - X) U_l(K_1, K_\nu, K_1) \quad (2.31)$$

and the second is the exchange term

$$\alpha_{\text{Fock}}\{U_l\}(K_1) = -\frac{\Lambda}{(2\pi)^2} \sum_{\nu=+,-} \int \frac{ds_\nu}{v_\nu} T \sum_{\omega_n} G_l(K_\nu) \frac{1}{2} (1 - X) U_l(K_\nu, K_1, K_1). \quad (2.32)$$

The third term is added to cancel the chemical potential renormalization due to the homogeneous part of the direct term

$$\alpha_\mu^{\text{hom.}}(l) = -\frac{1}{(2\pi)^2} \int d^2 k_1 \beta^{-1} \sum_{\omega_{n1}} \alpha_{\text{Hartree}}\{U_l\}(K_1). \quad (2.33)$$

If the initial interaction has no dynamics, the first nontrivial contributions to the flow of the selfenergy comes from the *renormalized* and not the bare interaction. As the interaction is renormalized by one-loop processes this implies that the interesting part of the flow of $\Sigma_l(K)$ is given by two loops. On the level of the present one-loop calculation it is thus consistent to neglect selfenergy corrections. This is what we do in the subsequent one-loop renormalization of the Hubbard model.

III. RENORMALIZATION GROUP FOR THE HUBBARD MODEL

In this section we will apply the above renormalization-group procedure to the Hubbard model. The model is given by equations (2.1), (2.2), and (2.3). The initial action S for the Hubbard model is given by expression (2.5), with the dispersion (2.3) and with the initial interaction $U_0 = \text{constant}(K_1, K_2, K_3)$. The interaction will depend more and more on (K_1, K_2, K_3) as we go on with the renormalization (as l increases) so that we will see at work the functional aspect of our renormalization group. We will complete our analysis by the renormalization of two-particle correlation functions.

A. Renormalization of the interaction

If we neglect the selfenergy corrections, the flow of the effective interaction is completely determined by the expressions (2.25-2.29) with the bare propagators instead of the renormalized ones:

$$G_l(K) \rightarrow G_0(K) \equiv (i\omega_n - \xi_{\mathbf{k}})^{-1} \quad (3.1)$$

The effective interaction is a function of three energy-momenta. This makes formulae (2.28) and (2.29) very complicated. For that reason we will consider only the marginal part of the dependence of U_l on energy-momenta. This approximation is justified by the zero-order scaling and power-counting arguments.^{22,23,30} For example, in one dimension this procedure justifies the well-known g-ology model¹⁵: one adds an index i to the electrons so that all electrons moving to the left have $i = -$ and all right-movers have $i = +$. Then the marginal interactions do not depend on impuls k and energy ω of the electrons in interaction, but only on their indices i . This can be seen as parametrization of the interactions as if the electrons were on the Fermi surface (or points in 1D) with $\omega = 0$. In two dimensions the marginal interactions depend only on polar coordinates of the wave vectors. Only the interactions between electrons at the Fermi surface are then kept and, if the Fermi surface is not nested, one gets the LEEA for the Fermi liquid.^{23,30}. The marginal processes in that case are

$$V(\theta_1, \theta_2) = U_l(K_1, -K_1, K_2) ; \omega_{1,2} = 0 ; \xi_{\mathbf{k}_{1,2}} = 0 \quad (3.2)$$

and

$$F(\theta_1, \theta_2) = U_l(K_1, K_2, K_1) ; \omega_{1,2} = 0 ; \xi_{\mathbf{k}_{1,2}} = 0. \quad (3.3)$$

V is the pairing amplitude and F is the forward scattering related to the Fermi liquid parameter. Both kinds of processes are shown in figure 6 for the case of the Hubbard model far from the half filling. We have analyzed in detail

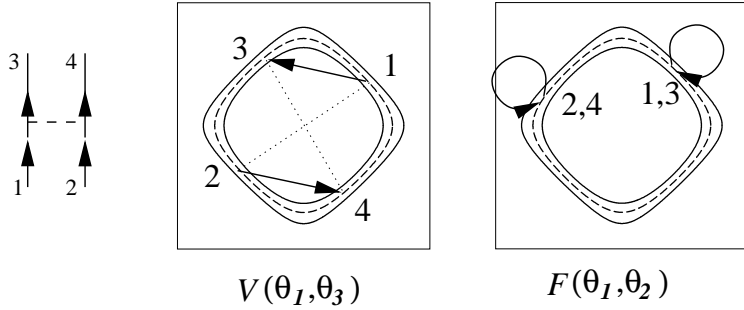


FIG. 6. The marginal interactions in the BCS regime.

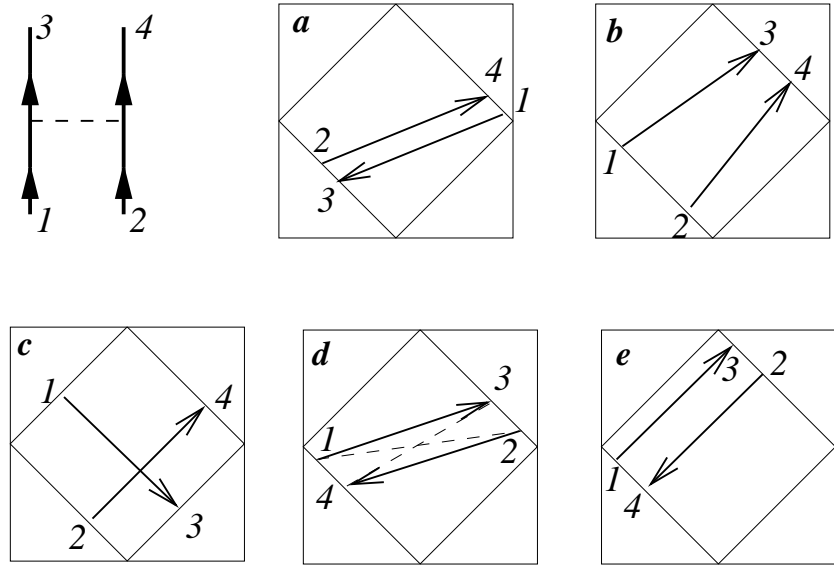


FIG. 7. Some of the marginal processes for the square Fermi surface.

this problem in a former article.²² Let us now concentrate on the square Fermi surface, for the half filled Hubbard model. The processes between electrons on the Fermi surface are now labeled with three variables instead of two as in the case of the Fermi surface without nesting : if we put particles 1, 2 and 3 *anywhere* on one side or on two opposite sides of the square, the fourth falls exactly on the square as well. This is due to the perfect flatness of the Fermi surface and to the marginality of the umklapp processes. A few examples of marginal interactions between the electrons on the square are shown on figure 7. The interaction depends only on the positions of the particles on the square. The “angle” θ can be defined in a way shown on figure 8. It is important to notice that even if the filling is not exactly one-half (and the Fermi surface not exactly square), all above interactions will still be important, as long as the effective phase space is open i.e. when $\Lambda > |\mu|$ (as on figure 8). We thus take as marginal all effective interactions viewed as functions of three angles θ of the particles:

$$U_l(K_1, K_2, K_3) \rightarrow U_l(\theta_1, \theta_2, \theta_3) ; \omega_{1,2,3,4} = 0 ; 1, 2, 3, 4 \text{ are on the square.} \quad (3.4)$$

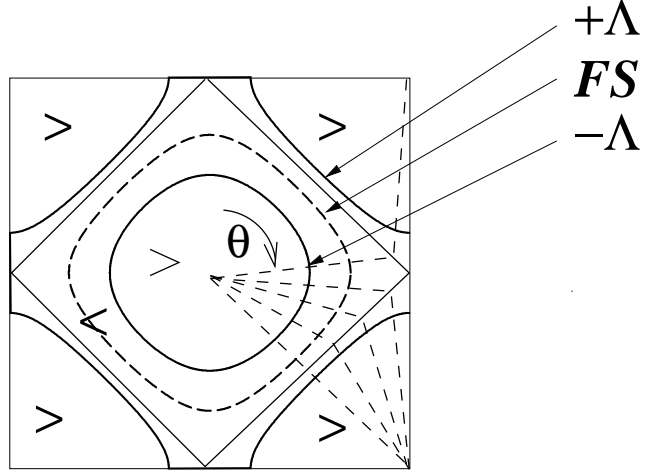


FIG. 8. The organization of the mode elimination. Dashed lines are the lines of constant “angle” θ .

When the cutoff becomes smaller than the chemical potential, we are back to the non nested case, in which the functions V and F are the marginal interactions. They read

$$V_l(\theta_1, \theta_2) = U_l(\theta_1, \theta_1 + \pi, \theta_2), \quad F_l(\theta_1, \theta_2) = U_l(\theta_1, \theta_2, \theta_1). \quad (3.5)$$

Altogether, for the half and almost half filled Hubbard model the function $U_l(\theta_1, \theta_2, \theta_3)$ given by (3.4) contains all marginal scattering processes. The renormalization group analysis is now much simpler because we deal with a function of three variables instead of six.

We will now derive the flow equation for $U_l(\theta_1, \theta_2, \theta_3)$ at zero temperature. The pleasant aspect of the Kadanoff–Wilson–Polchinski mode elimination technique at $T = 0$ is that Λ can then be interpreted as the temperature. Namely, the interaction at some temperature T is renormalized mainly by virtual processes involving “quantum” electrons, those with energy larger than T , having almost the distribution of the $T = 0$ electrons. This is exactly what we do with the renormalization group: only modes with $|\xi_{\mathbf{k}}| > \Lambda$ are involved in the virtual processes renormalizing U_l . Consequently, Λ is not only the measure of how many electrons are already integrated out : it has a *physical* meaning of the effective temperature.

Replacing $G_l(K)$ by $G_0(K)$ and $U_l(K_1, K_2, K_3)$ by $U_l(\theta_1, \theta_2, \theta_3)$ in expressions (2.28) and (2.29), we can get interactions out of Matsubara summations and perform the summations analytically. After taking the $T \rightarrow 0$ limit we obtain

$$\begin{aligned} \Xi\{U, U\}(\theta_1, \theta_2, \theta_3) &= \frac{-2}{(2\pi)^2} \sum_{\nu=+,-} \int d\theta \mathcal{J}(\nu\Lambda, \theta) \frac{\Theta(\nu\xi_{\mathbf{k}_\nu - \mathbf{q}_{pp}}) \Theta(|\xi_{\mathbf{k}_\nu - \mathbf{q}_{pp}}| - \Lambda)}{1 + \frac{\nu}{\Lambda} \xi_{\mathbf{k}_\nu - \mathbf{q}_{pp}}} \times \\ &\times U_{l_{pp}}(\theta_1, \theta_2, \theta) U_{l_{pp}}(\theta_3, \theta_4, \theta), \end{aligned} \quad (3.6)$$

$$\Pi\{U_1, U_2\}(\theta_1, \theta_2, \theta_3) = \frac{2}{(2\pi)^2} \sum_{\nu=+,-} \int d\theta \mathcal{J}(\nu\Lambda, \theta) \frac{\Theta(-\nu\xi_{\mathbf{k}_\nu + \mathbf{q}_{ph}}) \Theta(|\xi_{\mathbf{k}_\nu + \mathbf{q}_{ph}}| - \Lambda)}{1 - \frac{\nu}{\Lambda} \xi_{\mathbf{k}_\nu + \mathbf{q}_{ph}}} \times$$

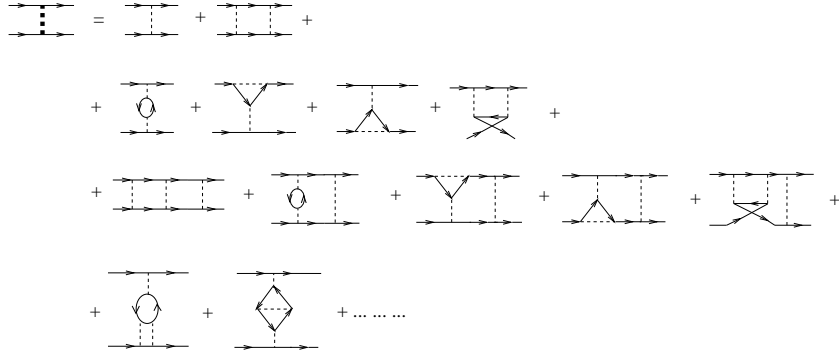


FIG. 9. The parquet summation.

$$\times U_{1,l_{ph}}(\theta_1, \theta, \theta_3) U_{2,l_{ph}}(\theta_4, \theta, \theta_2) . \quad (3.7)$$

\mathbf{k}_ν is the momentum of a particle at the angle θ with energy $\xi = \nu \Lambda$. $\mathcal{J}(\epsilon, \theta) \equiv J[(x, y)/(\epsilon, \theta)] = \partial s / \partial \theta / v(\theta, \epsilon)$ is the Jacobian of the transformation from rectangular coordinates in momentum space to polar coordinates. One should not forget that the scales l_{pp} and l_{ph} , which make the flow equation non-local, depend on external momenta and on the integration variable θ through \mathbf{q}_{pp} , \mathbf{q}_{ph} and \mathbf{k}_ν as given by the relations (2.22, 2.23). U_1 and U_2 represent U or XU as required by equation (2.25). Equation (3.6) gives the leading logarithmic flow in the p-p channel for the configuration of momenta with $\mathbf{q}_{pp} = 0$ while equation (3.7) gives the leading logarithmic flow in the p-h channel only exactly at half filling for $\mathbf{q}_{ph} = (\pi, \pi)$. In the standard renormalization-group procedure³⁰, only these configurations are taken into account. We see that in our formalism they are taken into account on equal footing with all other scattering processes, with any values of \mathbf{q}_{pp} and \mathbf{q}_{ph} , as illustrated on figure 7. The processes with the leading logarithmic renormalization in one channel and with less strong but still important flow in the other channel (as the processes in figures 7(d) and (e)) are the processes which couple strongly both renormalization channels. For example, the process in figure 7(d) has leading logarithmic renormalization in p-p channel and less strong (but still logarithmic!, because of partial nesting) renormalization in p-h channel, while the process in figure 7(e) has perfect nesting and, consequently, leading logarithm in p-h channel and weaker logarithmic flow in p-p channel.

If we want to see which series of diagrams is generated by our renormalization group we have to solve the differential equation (2.25) for U_l in iterations of the bare interaction U_0 . The obtained series is exactly the parquet summation. It is constructed from all iterations of five basic loop diagrams from figure 4(c). A few lowest order parquet diagrams are shown on figure 9.

An important aspect of the non half filled Hubbard model is that it can not be solved by a scale invariant renormalization group. The finite chemical potential determines the intrinsic scale, the physical interpretation of which is the crossover between two different renormalization regimes. The crossover can be seen from the *explicit* scale dependence of p-p and p-h differential loops $\Xi(l)$ and $\Pi(l)$. We can define the quantities

$$\beta_{pp}^0(l) = \Xi_l\{1, 1\}_{q_{pp}=0}, \quad (3.8)$$

$$\beta_{ph}^0(l) = \Pi_l\{1, 1\}_{\mathbf{q}_{ph}=(\pi, \pi)} . \quad (3.9)$$

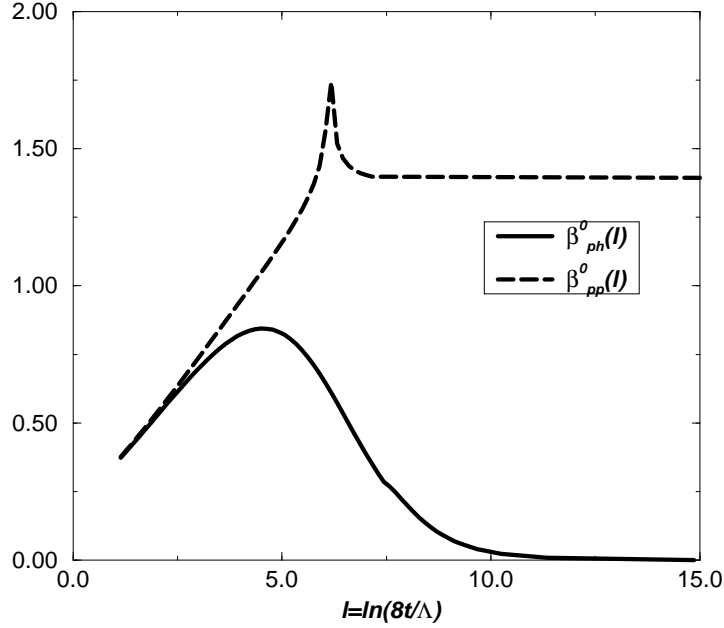


FIG. 10. The quantities $\beta_{pp}^0(l)$ and $\beta_{ph}^0(l)$. The crossover is at $l = l_\mu = 6$

They measure respectively the dominant parts of p-p and p-h renormalization tendencies. The configurations of momenta are chosen to give the most important flow : for the p-p channel at zero total momentum and for the p-h channel at the antiferromagnetic wave vector. The quantities $\beta_{pp}^0(l)$ and $\beta_{ph}^0(l)$ are shown in the figure 10 for finite chemical potential $\mu = -\Lambda_0 \exp(-l_\mu)$. We see that for $l < l_\mu$ both differential loops have linear dependence in logarithmic variable l ; the total (integrated) loops are thus square logarithmic, as is known for the half filled band. When $l > l_\mu$ the function $\beta_{pp}^0(l)$ crosses over to constant which gives the logarithm of the Cooper bubble. $\beta_{ph}^0(l)$ decays exponentially as $\exp(-2l) \sim \Lambda^2$: the nesting does not exist any more and the p-h flow crosses over to irrelevance. We call the first regime the parquet regime because both loops are important. The second regime, in which only the Cooper channel flows, we call BCS regime. The topology of the effective phase space in the parquet regime is open (see figure 8) and, in BCS regime, the phase space is a regular closed ring around the Fermi surface, as on figure 6. The peak of $\beta_{pp}^0(l)$ at $l = l_\mu$ is the enhancement due to van Hove singularity. The peak does not exist in $\beta_{ph}^0(l)$ because of the Θ -function constraint in (3.7). As we will see later, the renormalization in the parquet regime will give rise to precursors of a strong coupling fixed point with dominant antiferromagnetic correlations while in the BCS regime only a Cooper-like instability is possible.

It is difficult to read from the sole flow of the interaction U_l , what kind of correlations are enhanced and possibly divergent. For that purpose we have to calculate the renormalization of the correlation functions.

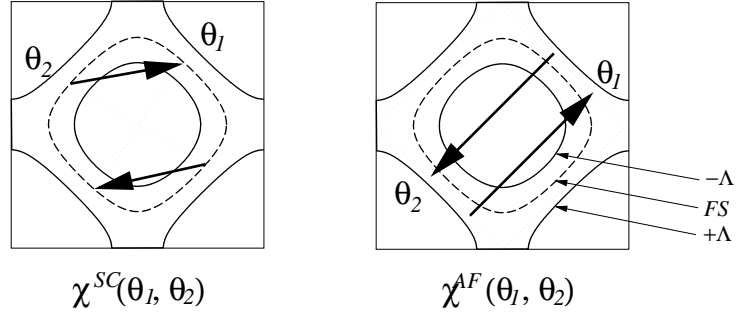


FIG. 11. The angle-dependent correlation functions.

B. Renormalization of the correlation functions

It is well known^{22,23,30,36} that, in studying the anisotropic superconductivity, one has to consider the pairing amplitude as a function of two angles, $V(\theta_1, \theta_2)$. The angles determine the angular positions of the Cooper pairs annihilated (θ_1) and created (θ_2) in the scattering. This interaction will be intimately related to the superconducting correlation function $\chi^{SC}(\theta_1, \theta_2)$. In the same spirit we can define the correlation function for the antiferromagnetism dependent on two angles. We will define both correlation functions in the following way

$$\begin{aligned} \chi_{\mathbf{q}}^{\delta}(\theta_1, \theta_2; |\tau_1 - \tau_2|) \\ = \int_{>} d\epsilon_1 \int_{>} d\epsilon_2 \mathcal{J}(\epsilon_1, \theta_1) \mathcal{J}(\epsilon_2, \theta_2) \langle \hat{\Delta}_{\mathbf{q}}^{\delta}(\epsilon_1, \theta_1; \tau_1) \hat{\Delta}_{\mathbf{q}}^{\delta}(\epsilon_2, \theta_2; \tau_2) \rangle, \end{aligned} \quad (3.10)$$

with $\delta = SC, AF$ (“superconductivity” or “antiferromagnetism”). The symbols “ $>$ ” mean that the energy integrations run over energies *outside* of the shell $\pm \Lambda$. Consequently, χ^{SC} and χ^{AF} are interpreted as the susceptibilities at the temperature $T = \Lambda$. They measure the response of outer shell electrons for given Λ . The order parameter variables are

$$\hat{\Delta}_{\mathbf{q}}^{SC}(\epsilon, \theta; \tau) \equiv \sum_{\sigma} \sigma \Psi_{\sigma, \mathbf{k}}(\tau) \Psi_{-\sigma, -\mathbf{k} + \mathbf{q}}(\tau), \quad (3.11)$$

$$\hat{\Delta}_{\mathbf{q}}^{AF}(\epsilon, \theta; \tau) \equiv \sum_{\sigma} \bar{\Psi}_{\sigma, \mathbf{k}}(\tau) \Psi_{-\sigma, \mathbf{k} + (\pi, \pi) + \mathbf{q}}(\tau), \quad (3.12)$$

where \mathbf{k} is given by the angle θ and the energy ϵ . The figure 11 illustrates what configurations of four angles are described by the correlation functions $\chi^{SC}(\theta_1, \theta_2)$ and $\chi^{AF}(\theta_1, \theta_2)$: the first measures the correlation of one cooper pair at θ_1 with the other at θ_2 and the second represents the correlation of the momentum (π, π) p-h pair at θ_1 with the other p-h pair at θ_2 . The correlation functions can be seen as response functions of the system to an infinitesimal external field, as was done by Bourbonnais and Caron¹⁶ in one dimension. We will generalize this procedure to two dimensions. We add to the action $S_{l=0}$ the term

$$S\{h\}_{l=0} = \int d\tau \int d\mathbf{q} \int d\theta \left[\int d\epsilon \mathcal{J}(\epsilon, \theta) \hat{\Delta}_{\mathbf{q}}^{\delta}(\epsilon, \theta; \tau) \right] \bar{h}_{\mathbf{q}}^{\delta}(\theta; \tau) + \text{h.c.} \quad (3.13)$$

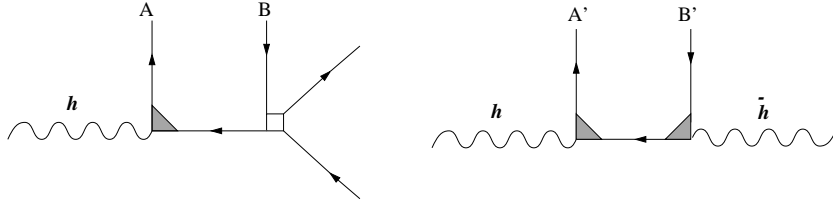


FIG. 12. Tree diagrams containing the source fields for AF.

The external angle dependent fields $\bar{h}_\mathbf{q}^\delta(\theta; \tau)$ are the source fields coupled to the order parameter variables of the type δ . The correlation functions (3.10) are obtained as

$$\chi_{l\mathbf{q}}^\delta(\theta_1, \theta_2; |\tau_1 - \tau_2|) = - \left[\frac{\delta^2 \ln Z}{\delta h_\mathbf{q}^\delta(\theta_1; \tau_1) \delta \bar{h}_\mathbf{q}^\delta(\theta_2; \tau_2)} \right]_{h, \Psi_<, \bar{\Psi}_<=0}. \quad (3.14)$$

Putting slow modes to zero means symbolically that we want the response only from the fast modes, as defined in equation (3.10). We consider only the static and long-wavelength limit. For that reason we will simply write $\chi(\theta_1, \theta_2)$ instead of $\chi_{\mathbf{q}=\mathbf{0}}(\theta_1, \theta_2; i\omega = 0)$ and $h(\theta)$ instead of $h_{\mathbf{q}=\mathbf{0}}(\theta; i\omega = 0)$. The correlations with the nonzero \mathbf{q} and ω are related to the dynamics of the collective modes, a problem which we do not study in this work.

We now apply the Kadanoff-Wilson-Polchinski formalism to the action containing terms (3.13). The procedure of collecting differential cumulants is analogous to what we explained in previous section, but now we treat $S\{h\}$ terms together with the interaction part S_I . To obtain the correlation functions for $h \rightarrow 0$, it is sufficient to follow the renormalization of the first two terms in powers of h in the h -dependent part of the effective action. They read:

$$\begin{aligned} S\{h\}_l = & \oint d\theta_1 \oint d\theta_2 \left[\int_0^{\Lambda(l)} d\epsilon \mathcal{J}(\epsilon, \theta_1) \hat{\Delta}_\mathbf{q}^\delta(\epsilon, \theta_1; \tau) \right] z_l^\delta(\theta_1, \theta_2) \bar{h}^\delta(\theta_2) + \text{h.c.} + \\ & + \oint d\theta_1 \oint d\theta_2 \bar{h}^\delta(\theta_1) \chi_l^\delta(\theta_1, \theta_2) h^\delta(\theta_2) + \text{tree terms}\{h\bar{h}\}. \end{aligned} \quad (3.15)$$

The term with $\chi_l^\delta(\theta_1, \theta_2)$ contains no electronic variable: it results from the elimination of all outer-shell electrons. From the definition (3.14) one can see that $\chi_l^\delta(\theta_1, \theta_2)$ is just the susceptibility of type δ . The “tree terms” are the terms containing one outer-shell contraction, two slow-electron fields and fields h and \bar{h} . They are illustrated by figure 12 for the AF channel. The square symbolizes the effective interaction for antiferromagnetism V_l^{AF} . We obtain it from the spin-spin interaction U_σ (see appendix A) putting the particles 1 and 3 on the opposite sides of the square Fermi surface so that $\mathbf{k}_1 - \mathbf{k}_3 = (\pm\pi, \pm\pi)$ (as on figure 11):

$$V_l^{AF}(\theta_1, \theta_2) = -(XU)(\theta_1, \theta_2, \tilde{\theta}_1). \quad (3.16)$$

$\tilde{\theta}$ is a function of θ such that

$$\mathbf{k}(\theta) - \mathbf{k}(\tilde{\theta}) = (\pi, \pi), \quad (3.17)$$

\mathbf{k} being on the square Fermi surface. The tree terms for SC channel are analogous, but with different orientations of the arrows: in the vertex z_l^{SC} both arrows point outwards and in the vertex $\bar{z}l^{SC}$ both arrows point inwards. The corresponding interaction is the familiar effective Cooper amplitude V (3.5). All “tree terms” in equation (3.15) are produced by the tree term of the Polchinski equation applied to the action with the $S\{h\}_l$ terms.

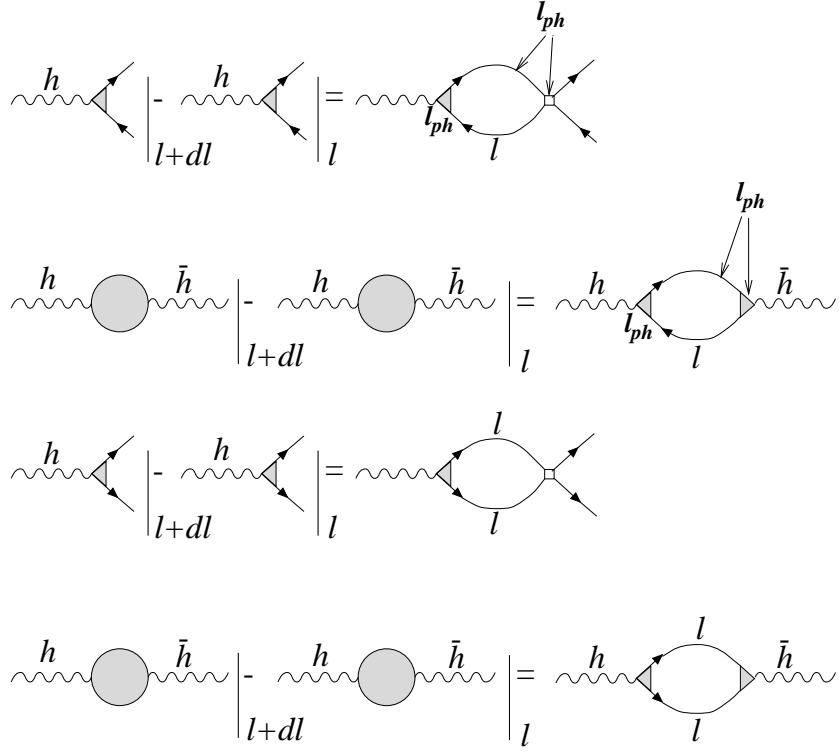


FIG. 13. The recursion relations for the vertices and for the correlation functions of the superconducting and of the antiferromagnetic type.

The coefficient $z_l^\delta(\theta_1, \theta_2)$ is the effective vertex of type δ . The equation (3.13) gives the initial conditions for z

$$z_{l=0}^\delta(\theta_1, \theta_2) = \delta_D(\theta_1 - \theta_2), \quad (3.18)$$

where δ_D is the Dirac function and for χ

$$\chi_{l=0}^\delta(\theta_1, \theta_2) = 0. \quad (3.19)$$

The differential flow of the triangular vertices z_l and of the correlation functions χ is obtained from the loop diagram of the Polchinski equation applied to the tree terms in the action $S\{h\}_l$. For the AF channel the, cumulant with on-shell integration of the electrons A and B on figure 12 gives the contributions to the vertex z_l^{AF} and the cumulant with electrons A' and B' on the shell contributes to the susceptibility χ_l^{AF} . A similar construction yields the renormalization of the vertex and of the susceptibility for the superconductivity. The resulting diagrams for the differential recursion relations for both channels are shown on figure 13. The corresponding flow equations write

$$\dot{z}_l^\delta(\theta_1, \theta_2) = - \oint d\theta z_{l_\delta}^\delta(\theta_1, \theta) D_l^\delta(\theta) V_{l_\delta}^\delta(\theta, \theta_2) \quad (3.20)$$

and

$$\dot{\chi}_l^\delta(\theta_1, \theta_2) = \oint d\theta z_{l_\delta}^\delta(\theta_1, \theta) D_l^\delta(\theta) z_{l_\delta}^\delta(\theta, \theta_2) \quad (3.21)$$

The scales l_{SC} and l_{AF} symbolize the scales l_{pp} and l_{ph} given by expressions (2.22) and (2.23), with the total momentum $\mathbf{q}_{pp} = 0$ and with the momentum transfer $\mathbf{q}_{ph} = (\pi, \pi)$ (antiferromagnetic wavevector):

$$l_\delta = \begin{cases} l_{pp}|_{\mathbf{q}_{pp}=0} = 0 & \text{for } \delta = \text{SC} \\ l_{ph}|_{\mathbf{q}_{ph}=(\pi,\pi)} = \ln \frac{\Lambda_0}{\Lambda_l + 2|\mu|} & \text{for } \delta = \text{AF} \end{cases}$$

We see that the renormalization of the antiferromagnetic correlation function is non-local in l if the filling is not exactly one-half. The function $D_l^\delta(\theta)$ is

$$D_l^{SC}(\theta) = \frac{1}{2} \sum_{\nu=+,-} \mathcal{J}(\nu \Lambda(l), \theta) \quad (3.22)$$

for the superconducting channel and

$$D_l^{AF}(\theta) = \frac{1}{2} \frac{\mathcal{J}(-\Lambda(l), \theta)}{1 + |\mu|/\Lambda(l)}, \quad (3.23)$$

for the antiferromagnetism where only the negative shell ($\nu = -1$) contributes to the flow. One sees that $D_l^{AF}(\theta)$ decays exponentially with l for $\Lambda \ll |\mu|$: in the BCS regime the correlation function for antiferromagnetism saturates with increasing l .

From the equations (3.20) and (3.21) we see that information about the *symmetry* of the correlations is determined from the symmetry of the effective interactions : functions $D_l^\delta(\theta)$ have a total lattice symmetry, but the interactions $V_l^\delta(\theta_1, \theta_2)$ can belong to any of the representations of the crystal symmetry group, in our case the D_4 point group. The decomposition of the interaction in terms of all basis functions of all irreducible representations of the D_4 group is discussed in detail in our previous paper.²² The diagonalization of the correlation functions $\chi_l^\delta(\theta_1, \theta_2)$ gives the final answer about which correlations are dominant in both AF and SC channels. The strength of the dominant correlations is associated to the maximal eigenvalues and the corresponding eigenvectors determine the symmetry and the form of the microscopic fluctuating field.

C. Discretization of renormalization group equations

The interaction U_l that we want to renormalize is a function of three continuous angular variables θ_1 , θ_2 and θ_3 . The beta function given by the equations (2.25-2.27, 3.6, 3.7) is a complicated function bilinear in U , and it does not seem possible to find an analytic solution for the flow of the interaction. We thus use numerical method. For that purpose we cut the Brillouin zone in m_i angular (θ) patches (see figure 8) and we assume that the interaction is a function only of the patch indices (i_1, i_2, i_3) of the three angles θ_1 , θ_2 and θ_3 . After the discretization of the interaction function the differential loops Ξ and Π become also functions of three indices:

$$\Xi\{U, U\}(i_1, i_2, i_3) = \sum_{i=0}^{m_i} B_{pp}(i_1, i_2, i; l) U_{l_{pp}}(i_1, i_2, i) U_{l_{pp}}(i_3, i_4, i), \quad (3.24)$$

$$\Pi\{U_1, U_2\}(i_1, i_2, i_3) = \sum_{i=0}^{m_i} B_{ph}(i_1, i_3, i; l) U_{1, l_{ph}}(i_1, i, i_3) U_{2, l_{ph}}(i_4, i, i_2) \quad (3.25)$$

with

$$B_{pp}(i_1, i_2, i; l) = \frac{-2}{(2\pi)^2} \sum_{\nu=+,-} \int_{[i]} d\theta \mathcal{J}(\nu\Lambda, \theta) \frac{\Theta(\nu\xi_{\mathbf{k}_\nu - \mathbf{q}_{pp}}) \Theta(|\xi_{\mathbf{k}_\nu - \mathbf{q}_{pp}}| - \Lambda)}{1 + \frac{\nu}{\Lambda} \xi_{\mathbf{k}_\nu - \mathbf{q}_{pp}}} \quad (3.26)$$

and

$$B_{ph}(i_1, i_3, i; l) = \frac{2}{(2\pi)^2} \sum_{\nu=+,-} \int_{[i]} d\theta \mathcal{J}(\nu\Lambda, \theta) \frac{\Theta(-\nu\xi_{\mathbf{k}_\nu + \mathbf{q}_{ph}}) \Theta(|\xi_{\mathbf{k}_\nu + \mathbf{q}_{ph}}| - \Lambda)}{1 - \frac{\nu}{\Lambda} \xi_{\mathbf{k}_\nu + \mathbf{q}_{ph}}}. \quad (3.27)$$

The total momentum and the momentum transfer become discrete variables:

$$\mathbf{q}_{pp} = \mathbf{k}(i_1) + \mathbf{k}(i_2),$$

$$\mathbf{q}_{ph} = \mathbf{k}(i_1) - \mathbf{k}(i_3).$$

The integral $\int_{[i]}$ is over i -th angular sector.

For a given number m_i of patches the number of *coupling constants* is equal to the number of configurations of three indices for all four particles lying on the square Fermi surface. That is a very large number. However because of the symmetry many of the coupling constants are identical. The available symmetries are: (i) The symmetries of the D_4 point group (mirror, $\pi/4$ -rotations); (ii) Time inversion symmetry \mathcal{T} , exchanging particles with holes and vice versa (see appendix A); (iii) The exchange symmetry: it is allowed to exchange simultaneously (1,2) and (3,4) particles; (iv) The freedom of choice of the points at the edges of the Brillouin zone. Figure 14 illustrates some of the symmetry operations applied to one of the coupling constants. The same figure shows the relation between the number of patches and the corresponding number of different marginal coupling constants, and the list of the coupling constants for $m_i = 4$ and $m_i = 8$.

The renormalization of the interaction as a function of three angles is now represented by a set of coupled differential equations, one for each coupling constant. In the same way we discretize the correlation functions $\chi_l^\delta(\theta_1, \theta_2)$ and the vertices $z_l^\delta(\theta_1, \theta_2)$. The equations (3.20) and (3.21) become

$$\dot{z}_l^\delta(i_1, i_2) = - \sum_i z_{l_\delta}^\delta(i_1, i) \bar{D}_l^\delta(i) V_{l_\delta}^\delta(i, i_2) \quad (3.28)$$

and

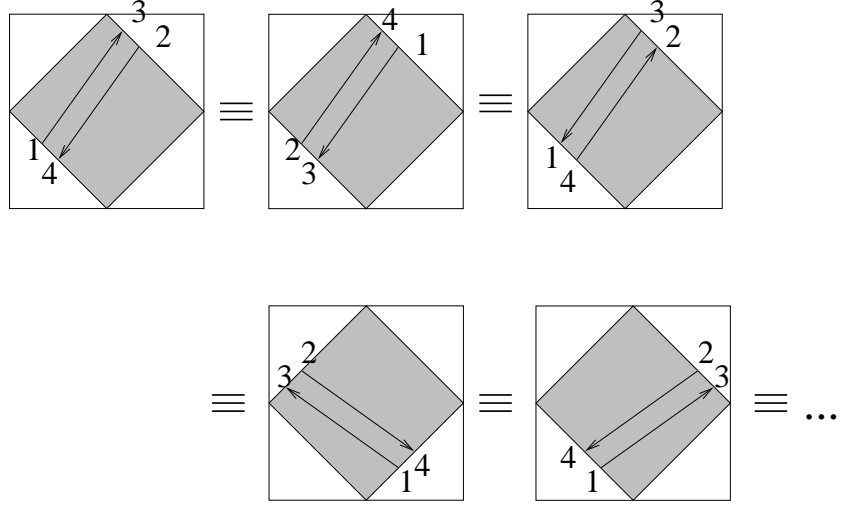
$$\dot{\chi}_l^\delta(i_1, i_2) = - \sum_i z_{l_\delta}^\delta(i_1, i) \bar{D}_l^\delta(i) z_{l_\delta}^\delta(i, i_2) \quad (3.29)$$

with

$$\bar{D}_l^\delta(i) \equiv \int_{[i]} d\theta D_l^\delta(\theta). \quad (3.30)$$

The initial conditions are the same as in the continuous case, provided we replaced the delta function by the Kronecker symbol divided by m_i :

$$\delta_D(\theta - \theta') \rightarrow \delta_{i,i'}/m_i.$$



m_i	no. of coupling const.
4	4
8	20
12	47
16	93
20	156
24	244
32	497

$m_i = 4$	$m_i = 8$
1 (0000)	1 (0000)
2 (0013)	2 (0015)
3 (0101)	3 (0026)
4 (0110)	4 (0101)
	5 (0110)
	6 (0125)
	7 (0152)
	8 (0202)
	9 (0211)
	10 (0220)
	11 (1111)
	12 (1133)
	13 (1155)
	14 (1313)
	15 (1331)
	16 (1357)
	17 (1375)
	18 (1515)
	19 (1537)
	20 (1551)

FIG. 14. The figure shows how we reduce the number of coupling constants by applying symmetry transformations. The dependence of the number of independent coupling constants on the number of angular patches m_i and the list of coupling constants for $m_i = 4$ and $m_i = 8$ are also shown.

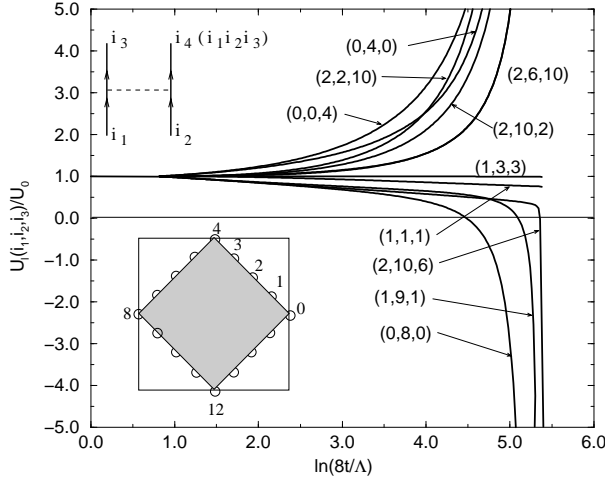


FIG. 15. The flow of a few typical (among 93) scattering amplitudes for a Fermi surface covered by 16 patches, for chemical potential $|\mu| = 8t \exp(-7.8)$ and initial interaction $U = 4t/3$.

D. Results and discussion

We have integrated numerically the renormalization equations for all coupling constants and for correlation functions and we have analyzed how the results change as functions of the initial interaction U_0 and of the chemical potential μ .

We first look at the renormalization flow of the coupling constants. Figure 15 shows the flow of several (among 93) coupling constants for a $M_i = 16$ -patches discretization; the choice of the input parameters is $U_0 = 4t/3$ and $l_\mu \equiv \ln 8t/|\mu| = 7.8$. The divergence happens at the critical scale $l_c \approx 5.3$. Approaching this point, some of the coupling constants increase and diverge, while some decrease and, after changing their sign, diverge to $-\infty$. Some do not change significantly upon renormalization and do not diverge. For example the coupling constant $U(0, m_i/2, 0)$ diverges very strongly to $-\infty$. It is a typical interaction with singular Cooper channel ($\mathbf{q}_{pp} = 0$) without nesting. Indeed, all coupling constants obeying only Cooper condition ($\mathbf{q}_{pp} = 0$) and without logarithmic flow in p-h channel diverge to $-\infty$. This is what we expected since the p-p channel “pushes” interactions downwards in a repulsive model. However, instead of just decaying to zero, they continue to decrease towards $-\infty$ because the Cooper amplitude obtains *attractive* components from p-h diagrams in, for example, the D-wave channel. The coupling constants with nesting between particles 1 and 3 or 1 and 4 diverge to $+\infty$. Among the interactions with nesting there are also umklapp processes like $(0,0,4)$ or $(2,2,10)$ in figure 15. The processes without divergence are those without any logarithmic instability neither from the nesting nor from the Cooper logarithm.

The critical scale l_c depends on the initial interaction and on the chemical potential. We associate the cutoff $\Lambda = \Lambda_0 \exp(-l_c)$ to the critical temperature T_c^{RG} . Figure 16 shows T_c^{RG} as a function of the chemical potential calculated for $m_i = 32$ patches (497 coupling constants). T_c^{RG} decreases rapidly but never really falls to zero : it becomes exponentially small far from half filling, the regime analyzed in ref. 22. Our numerical calculations show that

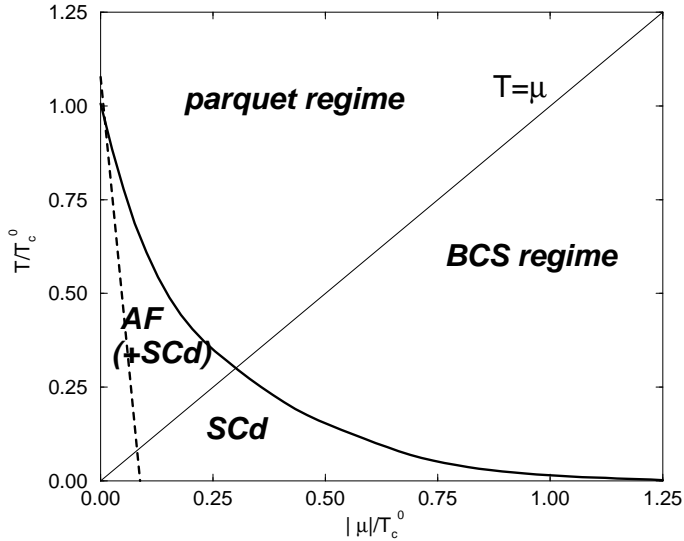


FIG. 16. The phase diagram. The solid line is the critical temperature T_c^{RG} and the dashed line is the temperature T_c^{MF} .

this form is universal if one measures μ in units of the critical temperature at half filling T_c^0 :

$$T_c^{RG} = T_c^0 \times f\left(\frac{|\mu|}{T_c^0}\right) \quad (3.31)$$

where f is the universal function visible on figure 16. Thus T_c depends on the interaction only through $T_c^0 \equiv 8t \exp(-l_c^0)$, where

$$(l_c^0)^2 = C \frac{4t}{U_0} \quad (3.32)$$

C being a numerical constant, $C \approx 8.8$. The dashed line in figure 16 represents the critical temperature T_c^{MF} that one obtains when taking into account only the last term of equation (2.25): $X\beta\{XU, XU\}$. This is the “renormalization group” version of the RPA summation, equivalent to the mean field for the antiferromagnetism. We see now the main difference between the critical temperature in the mean field approximation and the result obtained with the renormalization group: in the case of weak doping, because of the *destructive* interference between channels p-p and p-h, T_c^{RG} is slightly reduced with respect to T_c^{MF} . The ratio between the critical scales l_c^{RG} and l_c^{MF} (associated to RG and MF critical temperatures) do not depend on the interaction. Its value at half filling is $l_c^{MF}/l_c^{RG} = 0.985$, which is not far from the value 0.981, calculated by Dzyaloshinskii and Yakovenko using parquet equations.¹⁹ T_c^{MF} disappears completely at some threshold doping. This means that the physical mechanisms which reduce T_c^{RG} near half filling, at higher doping enhance T_c^{RG} keeping it always non-zero.

The straight line $T = \mu$ is roughly the crossover between the parquet and the BCS regimes. If the instability occurs in the parquet regime, both p-p and p-h correlations are strongly enhanced near T_c^{RG} . On the other hand, in the BCS regime only the p-p correlations are critical. To know which fluctuations are the most important at the instability, we need the renormalization of the correlation functions. However, there is a formal problem related to the fact that we are performing the renormalization at $T = 0$ and associating the cutoff to the temperature: the renormalization equations for the antiferromagnetic vertex (3.28) and the correlation function (3.29) ($\delta = AF$) are

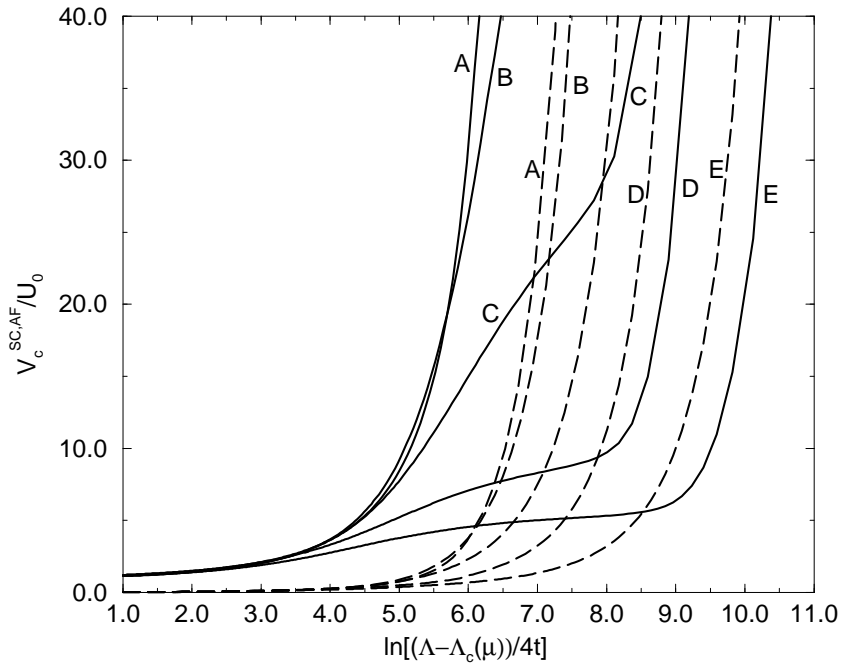


FIG. 17. The flow of V_c^{SC} (dashed line) and of V_c^{AF} (solid line) for $|\mu|/(4t) = 0$ (A); 0.00067(B); 0.0018(C); 0.0049(D); 0.0081(E).

retarded in l of a quantity $l - \ln \frac{\Lambda_0}{\Lambda_l + 2|\mu|}$. If the interaction V_l^{AF} diverges at $l = l_c$, the divergence of the function χ_l^{AF} will be retarded. Since we can not go further than $l = l_c$ in the renormalization this divergence can not be seen in the present formalism. The cure is to work at finite temperature. In that case one performs the full renormalization, up to $l = \infty$ and the final *fixed point* correlation functions are the ones at the given temperature. This is the procedure that we use in the following chapter.

However, in the zero temperature formalism one can still get some idea of what happens with different correlations at $l = l_c$: The finite cutoff divergence of the correlation functions for SC and AF are determined exclusively by the divergence of the effective interactions V_l^{SC} and V_l^{AF} . Furthermore the symmetry of the correlation functions is also brought only by the symmetry of the effective interactions. It is thus reasonable to assume that the dominant eigenvalue of the correlation function is driven mostly by the dominant attractive (negative) eigenvalue of the corresponding effective interaction. From the renormalization of the interaction (the set of coupling constants) we can deduce the flow of the effective interactions V_l^{SC} and V_l^{AF} as given by equations (3.5) and (3.16). The diagonalization is straightforward because both interactions are matrices whose rows and columns are labeled by discretized angular variables. Let's call the most attractive eigenvalues of V_l^{SC} and V_l^{AF} respectively V_c^{SC} and V_c^{AF} . Figure 17 shows the flow of V_c^{SC} and of V_c^{AF} near the critical point as a function of $\ln[(\Lambda - T_c^{RG}(\mu))/4t]$ for several values of the chemical potential. The critical temperature $T_c^{RG}(\mu)$ is adjusted for every value of μ . Solid lines represent the anti-ferromagnetic interaction V_c^{AF} . The corresponding eigenvector belongs to A_1 . It is a standard S-wave. The dashed lines represent the flow of V_c^{SC} . Its eigenvector belongs to the B_1 representation ($D_{x^2-y^2}$ -wave). Both coupling constants are always enhanced by the renormalization, which means that the correlation functions are always enhanced respectively to their value at $U_0 = 0$. The possibility of the charge density wave instability is excluded: we have

checked that all eigenvalues of the charge interactions U_c (see appendix A) at $2k_F$ decay upon renormalization. The competition between the divergences of V_c^{SC} and V_c^{AF} is clearly visible in the figure. At half filling the coupling V_c^{AF} diverges faster than V_c^{SC} . As the chemical potential increases, both divergences are weaker but in V_c^{AF} an inversion of the slope is visible. This is the signature of the crossover from the parquet to the BCS regime. At half filling this crossover does not exist and the slope of V_c^{AF} is always upwards. The lines labeled by (C) in the figure correspond to the critical temperature in the parquet regime. However, V_c^{AF} starts to “feel” the proximity of the crossover: the critical scale is $l_c = 6.025$ and the crossover occurs at about $l_x \sim l_\mu = 7$. The divergence of V_c^{AF} can still entail the divergence of the antiferromagnetic correlation function because the nesting is still relevant. The Cooper amplitude V_c^{SC} always has an upward slope and diverges at T_c^{RG} because the p-p channel has a logarithmic instability for any doping. Lines (D) and (E) are examples the flow in the BCS regime. After some saturation tendencies, V_c^{AF} still diverges at T_c^{RG} . This divergence is only due to the p-p loop: for a choice of angles θ_1 and θ_2 such that $\theta_2 = \theta_1 + \pi$, the function $V^{AF}(\theta_1, \theta_2) = V^{SC}(\theta_1, \tilde{\theta}_1)$, that diverge. The relation between θ_1 and $\tilde{\theta}_1$ is given by equation (3.17). The interaction V_c^{AF} is thus driven upwards by the Cooper channel. It has no effect on the correlation function for the antiferromagnetism because its flow has disappeared together with the nesting. This will become visible in the next section where we calculate the temperature dependence of both correlation functions near the critical temperature.

IV. FINITE TEMPERATURE RG

In the zero temperature formalism the flow of different quantities was of physical interest. In the finite temperature renormalization group, we are interested in the fixed point value of the correlation functions. The temperature is taken as input parameter. If T is larger than the critical cutoff Λ_c (called T_c^{RG} in the previous section), the divergence of the renormalization flow will disappear. Consequently we will be able to control the flow all the way down to the fixed point $\Lambda = 0$. In the zero temperature formalism the effects of the elimination of the slow modes are neglected. At finite temperature all modes are integrated so that contributions of the thermal electrons are also taken into account. The other advantage of the finite temperature renormalization group is that we can explicitly follow the temperature dependence of the correlation functions for the superconductivity and the antiferromagnetism.

Formally, the finite temperature procedure is the same as in the previous section with the difference that the differential loops Ξ and Π have to be calculated at finite temperature. They now write

$$\begin{aligned} \Xi\{U, U\}(T, \theta_1, \theta_2, \theta_3) \\ = \frac{-2}{(2\pi)^2} \sum_{\nu=+,-} \int d\theta \mathcal{J}(\nu\Lambda, \theta) \frac{[1 - f(\nu\Lambda) - f(\xi_{\mathbf{k}_\nu} - \mathbf{q}_{pp})] \Theta(|\xi_{\mathbf{k}_\nu} - \mathbf{q}_{pp}| - \Lambda)}{\nu + \frac{1}{\Lambda} \xi_{\mathbf{k}_\nu} - \mathbf{q}_{pp}} \\ \times U_{l_{pp}}(\theta_1, \theta_2, \theta) U_{l_{pp}}(\theta_3, \theta_4, \theta), \end{aligned} \quad (4.1)$$

$$\begin{aligned} \Pi\{U_1, U_2\}(T, \theta_1, \theta_2, \theta_3) \\ = \frac{2}{(2\pi)^2} \sum_{\nu=+,-} \int d\theta \mathcal{J}(\nu\Lambda, \theta) \frac{[f(\nu\Lambda) - f(\xi_{\mathbf{k}_\nu} + \mathbf{q}_{ph})] \Theta(|\xi_{\mathbf{k}_\nu} + \mathbf{q}_{ph}| - \Lambda)}{\nu - \frac{1}{\Lambda} \xi_{\mathbf{k}_\nu} + \mathbf{q}_{ph}} \\ \times U_{1,l_{ph}}(\theta_1, \theta, \theta_3) U_{2,l_{ph}}(\theta_4, \theta, \theta_2). \end{aligned} \quad (4.2)$$

The function $f(\epsilon)$ is the Fermi distribution at temperature T . The finite temperature version of the flow equations for the vertices z and for the correlation functions χ are again given by equations (3.20) and (3.21) but with modified D^{SC}

$$D_l^{SC}(T, \theta) = \sum_{\nu=+, -} \mathcal{J}(\nu\Lambda, \theta) \tanh\left(\frac{\nu\Lambda}{2T}\right) \quad (4.3)$$

and D^{AF}

$$D_l^{AF}(T, \theta) = \sum_{\nu=+, -} \mathcal{J}(\nu\Lambda, \theta) \frac{[f(\nu\Lambda) - f(2|\mu| - \nu\Lambda)] \Theta(|2|\mu| - \nu\Lambda| - \Lambda)}{2(\nu - \frac{|\mu|}{\Lambda})}. \quad (4.4)$$

We see that now both shells $\nu = +, -$ contribute to D_l^{AF} for $\Lambda > |\mu|$, unlike in the zero temperature case where $\nu = +$ contributions were forbidden by the Fermi distribution. In the discretized version of the flow equations, one calculates Ξ and Π from expressions (3.24) and (3.25), but with

$$\begin{aligned} B_{pp}(i_1, i_2, i; l, T) \\ = \frac{-2}{(2\pi)^2} \sum_{\nu=+, -} \int_{[i]} d\theta \mathcal{J}(\nu\Lambda, \theta) \frac{[1 - f(\nu\Lambda) - f(\xi_{\mathbf{k}_\nu - \mathbf{q}_{pp}})] \Theta(|\xi_{\mathbf{k}_\nu - \mathbf{q}_{pp}}| - \Lambda)}{\nu + \frac{1}{\Lambda} \xi_{\mathbf{k}_\nu - \mathbf{q}_{pp}}} \end{aligned} \quad (4.5)$$

and

$$\begin{aligned} B_{ph}(i_1, i_3, i; l, T) \\ = \frac{2}{(2\pi)^2} \sum_{\nu=+, -} \int_{[i]} d\theta \mathcal{J}(\nu\Lambda, \theta) \frac{[f(\nu\Lambda) - f(\xi_{\mathbf{k}_\nu + \mathbf{q}_{ph}})] \Theta(|\xi_{\mathbf{k}_\nu + \mathbf{q}_{ph}}| - \Lambda)}{\nu - \frac{1}{\Lambda} \xi_{\mathbf{k}_\nu + \mathbf{q}_{ph}}} \end{aligned} \quad (4.6)$$

The equations for finite temperature $z_l^\delta(T, i_1, i_2)$ and $\chi_l^\delta(T, i_1, i_2)$ are (3.28) and (3.29) with $D_l^\delta(T, i)$ calculated from (3.30), but using (4.3) and (4.4).

To find each point of the phase diagram, we have to find the fixed-point ($\Lambda \rightarrow 0$) value of the maximal eigenvalues $\chi_c^\delta(T, l)$ of the correlation functions $\chi_l^\delta(i_1, i_2)$; ($\delta = SC, AF$). It means that the complete renormalization from $l = 0$ to $l \rightarrow \infty$ has to be done for each temperature. The flow of the quantities $\chi_c^{SC}(T, l)$ and $\chi_c^{AF}(T, l)$ is shown in figure 18 for several temperatures and three different values of the chemical potential. The susceptibilities for the non-interacting ($U = 0$) case are also shown. For all calculations the initial interaction was $U_0 = 4t/3$ and we have cut the Brillouin zone into $m_i = 32$ patches. The symmetry of the dominant superconducting correlations is for all cases B_1 (which transforms as d_{x-y^2}) and the dominant antiferromagnetic correlations have A_1 (s) symmetry. They correspond to the symmetries of the strongest attractive components of the effective interactions $V^{SC, AF}$ found in the previous section.

Let's concentrate first on figure 18(a) that shows the flow at half filling. The entire flow is in the parquet regime: the nesting is perfect. In the beginning of the flow where $\Lambda_l \gg T$ all correlation functions, bare or with correlations, scale as if the temperature was zero, i.e. like $\ln^2(\Lambda_0/\Lambda) = l^2$. As the cutoff approaches the temperature, the flow starts to saturate. At the same time the effects of the interaction become more and more visible as we decrease the temperature. For all temperatures χ_c^{AF} and χ_c^{SC} are enhanced from their bare values χ_0^{AF} and χ_0^{SC} that are equal at half filling. As we approach the temperature $T \approx 0.0163$ from above, the difference between the bare and the interacting cases increases rapidly; we interpret this temperature as the critical temperature. We have approximated

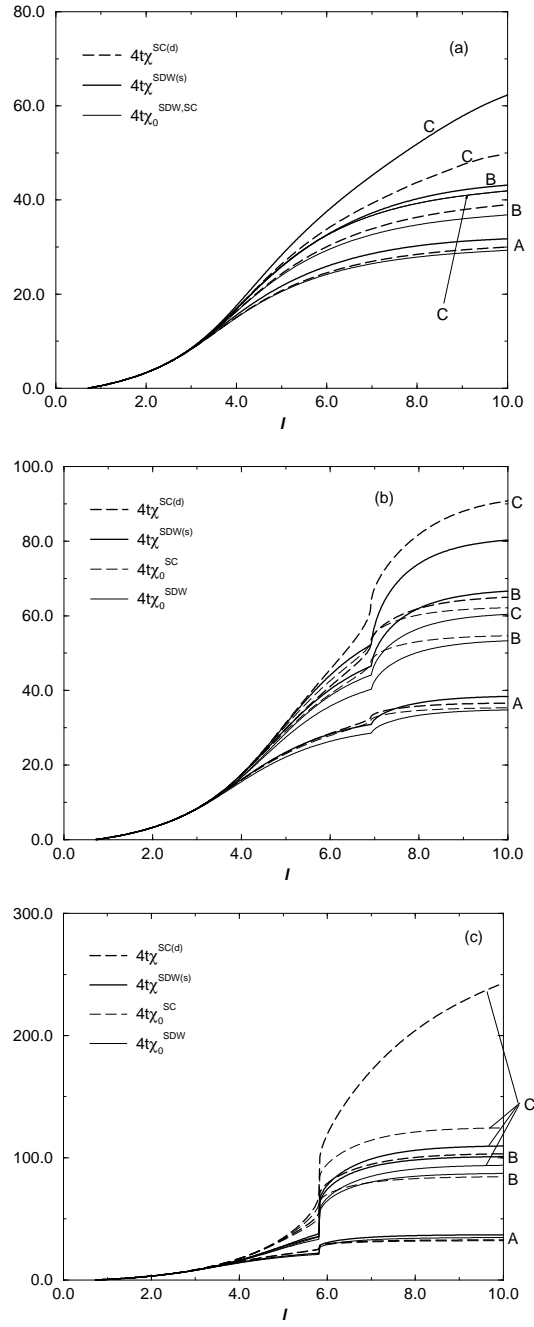


FIG. 18. The flow of the correlation functions with interaction (thick lines) and without interaction (thin lines) (a): at half filling for $T/4t = 0.03$ (A), 0.0204 (B), 0.0163 (C); (b): at $|\mu|/4t = 0.002$ for $T/4t = 0.0228$ (A), 0.0108 (B), 0.0086 (C); and (c): at $|\mu|/4t = 0.006$ for $T/4t = 0.03$ (A), 0.006 (B), 0.0026 (C).

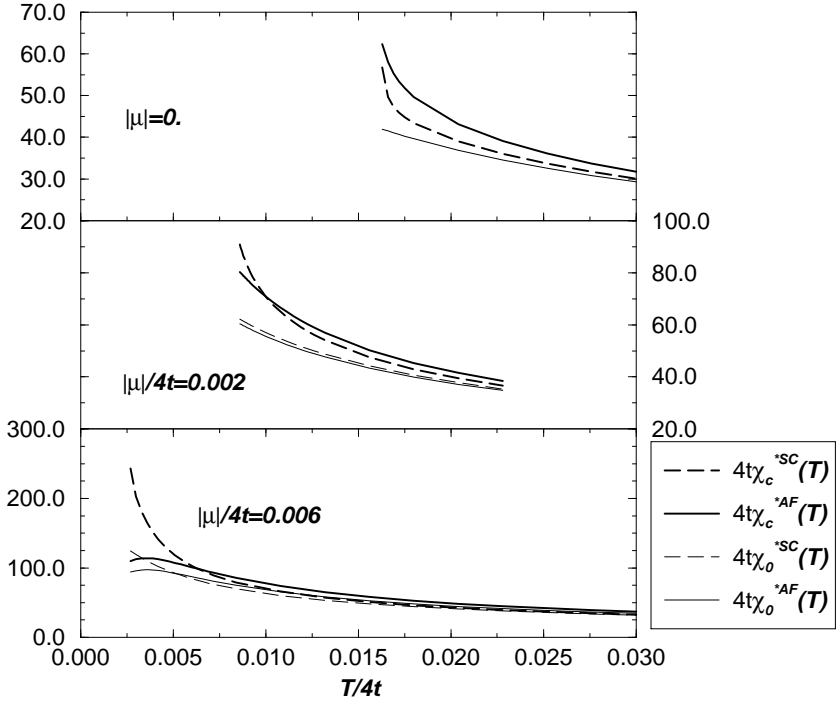


FIG. 19. The temperature dependence of the fixed-point correlation functions for three different values of the chemical potential.

the fixed point values $\chi_c^{*\delta}(T)$ and $\chi_0^{*\delta}(T)$ of $\chi_c^\delta(T, l)$ and $\chi_0^\delta(T, l)$ with their value for $l = 10$ (the corresponding energy Λ_l is much smaller than any physical energy scale). Figure 19(a) shows the temperature dependence of the fixed point values at half filling. The bare susceptibility scales as $\ln^2(\Lambda_0/T)$. The interaction makes both susceptibilities diverge, but the antiferromagnetic one diverges first.

Now we increase the chemical potential to $|\mu|/4t = 0.002$ (figure 18(b)). The beginning of the flow, where $\Lambda_l \gg |\mu|$, is still square-logarithmic. When l becomes close to $l_\mu = 6.9$ the bare antiferromagnetic correlations start to be weaker because we approach the crossover from the parquet to the BCS regime. The non-analytic point is at $l = l_\mu$; at this point the flow equations (3.28) and (3.29) have a peak because of the van Hove singularity in $D_l^\delta(\theta)$ at $\theta = 0, \pi/2, \pi, 3\pi/2$. Again, as we approach the critical temperature the effects of the interaction become stronger and stronger so that the difference between $\chi_c^\delta(T, l)$ and $\chi_0^\delta(T, l)$ increases more and more. The temperature dependence of the fixed point values for all correlation functions for the present case are shown in figure 19(b). The critical temperature is $T_c^{RG}/4t = 0.0075$, which is higher than $|\mu|/4t = 0.002$. This means that the instability is still in the parquet regime, but not too deep: the proximity of the crossover already affects the antiferromagnetic correlations which start to lose their strength with respect to the superconducting correlations near the instability. However, both are still strongly enhanced and their flow is dominated by the parquet part ($l < l_\mu$) for all temperatures $T > T_c^{RG}$.

Let's increase further the chemical potential to $|\mu|/4t = 0.006$ (figure 18(c)). The flow of the antiferromagnetic correlations saturates in the BCS regime ($l > l_\mu = 5.8$), but both correlation functions SC and AF remain enhanced from their bare values. In the temperature dependence of their fixed point values (figure 19(c)) one sees that only the superconducting instability is possible. The critical temperature is lower than the chemical potential, i.e. the

instability is in the BCS regime, in which the p–h part of the flow is negligible. The antiferromagnetic susceptibility even starts to decrease with the temperature when $T \lesssim \mu$. This happens because we do not adjust the wave vector of the SDW to the best nesting (incommensurate SDW) but we keep it for simplicity at (π, π) . Nothing drastic would happen even if we have taken small deviations of the best nesting wave vector from (π, π) : the susceptibility would saturate as the temperature decreases because the differential p–h bubble decays in the BCS regime *at any wave vector* with positive power of Λ .

The universal function $f(|\mu|/T_c^0)$ (equation 3.31), which determines the dependence of the critical temperature on the chemical potential, is practically the same as the one obtained in the zero temperature formalism. The final phase diagram is the one on figure 16. At half filling the antiferromagnetic fluctuations are dominant over the superconducting ones but both correlation functions diverge at the critical temperature. Upon doping the antiferromagnetic correlations loose their strength while the superconducting correlations remain strongly divergent. The divergence of AF correlation functions is completely suppressed if the critical temperature is in the BCS regime.

V. CONCLUSION

We have formulated the exact Kadanoff–Wilson–Polchinski (KWP) renormalization group for a general problem of interacting fermions on a two–dimensional lattice. In principle the generalization to higher dimensions is trivial. The procedure of the KWP renormalization scheme is to integrate out successively the degrees of freedom starting from high energies and to follow the renormalization of *all* terms in the effective action. We parametrize the renormalization by a high–energy cutoff $\Lambda \equiv \Lambda_0 \exp(-l)$ determining the ring $\pm\Lambda$ around the Fermi surface. In order to take the whole Brillouin zone into account, the cutoff Λ is taken to be equal to the bandwidth ($\Lambda_0 = B.W.$) at the beginning of the renormalization ($l = 0$) . As one proceeds with the mode elimination, vertices of all orders are created. To follow the exact renormalization of the effective action we need to know the flow (the dependence on l) of all vertices. The Polchinski equation (equations 2.16, 2.17 and figure 3) determines the differential flow of all vertices as *functions* of energy–momenta. In principle the fixed point solution ($l \rightarrow \infty$) of this equation gives us the exact connected Green functions of the model.^{31,32} Clearly, the exact integration of Polchinski equation is impossible and for concrete calculations we have to truncate the effective action.

The truncation at the sextic term (at the three–particle interaction term) generates the one–loop renormalization group for the two–body interaction. The truncated effective action is given by expression (2.21). Its renormalization is determined by the flow equation for the two–body interaction and for the self–energy. The flow equation for the interaction U_l is made of all one–loop diagrams bilinear in U_l as shown on figure 4 and by equation (2.25). Note that U_l is renormalized as a function of three energy–momenta (the fourth is conserved), i.e. this is a *functional* renormalization group. The β function (2.25) contains the contributions from the particle–particle (p–p) (β_{pp}) and the particle–hole (p–h) diagrams (β_{ph}). The first term is called the BCS contribution in the literature, the next three terms are the zero sound (ZS) contribution, and the last term is the ZS’ contribution to the differential flow. The flow equation for the interaction is not local in l as one can see from equations (2.28) and (2.29) for differential p–p and

p-h bubbles: at some step l of the renormalization, U_l is renormalized by the values of U at former steps $l_{pp}(\mathbf{k}, \mathbf{k}_1, \mathbf{k}_2)$ and $l_{ph}(\mathbf{k}, \mathbf{k}_1, \mathbf{k}_3)$. This non-locality is the price we have to pay if we want to keep all contributions, logarithmic or not, that renormalize the interaction. In this way one takes correctly into account, for example, the p-h flow because of the imperfectly nested Fermi surface. The standard (local) Wilsonian RG³⁰ that takes into account only dominant logarithmic diagrams (those with $l = l_{pp} = l_{ph}$) can give useful results only for the perfectly nested (but not square) Fermi surfaces or the Fermi surfaces far from being nested, so that the p-h part is negligible.

We have applied the one-loop renormalization group to the Hubbard model on a square lattice near half filling. The interaction function U that we renormalize is dependent on the angular (θ) position of three momenta on the square Fermi surface (the fourth one is conserved). All radial momentum dependencies and energy (ω) dependencies are irrelevant to the Fermi liquid scaling. It is important that we allow variables θ of the interacting particles to be anywhere on the square Fermi surface and not only in the configurations which give perfect nesting or zero total momentum (see figure 7). This means that we do not limit ourselves to the leading logarithmic parts of the flow but that we take all non-logarithmic contributions into account.

From the explicit scale dependence of the differential flow for U we see two renormalization regimes (see figure 10). In the first regime, $\Lambda_l > |\mu|$. We call it the parquet regime because both p-p and p-h contributions are important. The other regime exists in the non-half filled case when $\Lambda_l < |\mu|$. There, only p-p loops have a strong logarithmic flow while the p-h part decays to zero. We call this regime the BCS regime. The effective phase space ($|\xi_0(\mathbf{k})| < \Lambda$) in the parquet regime is open so that the nesting is relevant (see figure 2), while in the BCS regime the phase space is a closed regular ring of degrees of freedom around the Fermi surface so that perfect nesting is impossible (see figure 6). The flow in the parquet regime is characterized by a strong coupling between the p-p and the p-h channels of renormalization. This coupling comes into play over the interactions that have a strong flow from both p-p and p-h diagrams. For the case of the (nearly) square Fermi surface these are all interactions between electrons from opposite sheets of the Fermi surface.

The leading correlations in the Hubbard model are expected to be antiferromagnetic and/or superconducting. To give a precise answer to this question, we use Kadanoff–Wilson–Polchinski procedure to construct the renormalization-group equations for the *angle resolved* correlation functions $\chi_l^{AF}(\theta_1, \theta_2)$ and $\chi_l^{SC}(\theta_1, \theta_2)$ for antiferromagnetism and superconductivity, defined by equation (3.10). At a given step $\Lambda(l)$ of the renormalization these correlation functions measure the linear response of the electrons outside the shell $\pm\lambda$ around the Fermi surface. We take the static long-wave limit. The renormalization equation for $\chi_l^{AF,SC}$ is (3.21). The renormalization of the correlation functions depends on the renormalization of the vertices $z^{AF,SC}$ (eq. 3.20). Furthermore, from equations (3.20) and (3.21) one sees that the flows of the susceptibilities and of the vertices depend on the flows of the corresponding *effective interactions* V_l^{SC} and V_l^{AF} , given by (3.5) and (3.16) respectively.

The flow equations for the interaction U_l (2.25), for the vertices $z_l^{SC,AF}$ (3.20) and for the correlation functions $\chi_l^{SC,AF}$ (3.21) can be integrated numerically if we discretize their θ -dependence. The coupling function is then approximated by a set of coupling constants. The vertices and correlation functions become discrete matrices. Using physical and geometrical symmetries we reduce number of the coupling constants to a set of the independent ones (see

figure 14). The functional renormalization–group equations become a set of equations, one for each coupling constant and for each matrix element of $z_l^{SC,AF}$ and $\chi_l^{SC,AF}$.

We have solved the renormalization equations for up to $m_i = 32$ angular patches. The typical flow of the coupling constants is shown on figure 15. There is a critical scale for which a large number of coupling constants diverge. We associate the corresponding cutoff to the critical temperature T_c^{RG} . Its dependence on the chemical potential is shown on figure 16 (solid line) together with the RPA result (dashed line). At the line $T_c^{RG}(\mu)$ the electronic correlations are strongly enhanced. The type and the form of the corresponding microscopical fluctuating fields are given by the dominating eigenvalues (and their eigenvectors) of the correlation matrices $\chi_l^{SC,AF}$. These are determined by the dominant attractive eigenvalues V_c^{SC} and V_c^{AF} of the effective interactions. For all values of the chemical potential studied in this work, the eigenvalue V_c^{SC} corresponds to $d_{x^2-y^2}$ (or B_1) singlet superconductivity while V_c^{AF} is an s–wave (A_1 representation). The flow of the interactions V_c^{SC} and V_c^{AF} in the vicinity of the critical point $\Lambda = T_c^{RG}$ is shown on figure 17. At half filling V_c^{AF} is dominant. Upon doping, the divergence of V_c^{AF} loses its strength and the divergence of V_c^{SC} becomes dominant.

To determine more precisely the dominant fluctuations near T_c^{RG} , we have done one further step in the renormalization–group formalism: we have introduced the temperature explicitly into the flow equations. In this formalism the cutoff Λ has no more a physical meaning of the effective temperature. At given temperature T the physical information is contained in the fixed point ($\Lambda \rightarrow 0$) of the correlation functions. This extension of the formalism was necessary because in the zero–temperature procedure it was not possible to have the divergence of χ_l^{AF} at the same scale l_c as the divergence of the coupling V^{AF} : for any nonzero chemical potential the flow of χ_l^{AF} has a finite retardation in l (see equations (3.20) and (3.21)). Thus χ_l^{AF} diverges later, at $l > l_c$. In the finite temperature formalism χ_l^{AF} , χ_l^{SC} , V_l^{AF} and V_l^{SC} all diverge at the same temperature. The price to pay is that for each temperature we have to integrate the complete flow all the way from $l = 0$ to $l = \infty$ and to follow how the result changes with the temperature.

The flow of the dominant eigenvalues of χ_l^{AF} and χ_l^{SC} at a few different values of the temperature is shown on figure 18 for three different values of the chemical potential. Both correlation functions are always enhanced with respect to their bare ($U = 0$) values. The temperature dependence of the fixed point correlation functions is shown on figure 19. The critical temperature T_c^{RG} found by the finite temperature method is practically the same as the one found by the zero–temperature calculations, but now we are able to follow explicitly the enhancement of the correlations of both types in the vicinity of the instability. It is clearly visible how the doping favors superconductivity and how the divergence of χ^{*AF} is completely suppressed if the instability is in the BCS regime, i.e. if $T_c^{RG} < |\mu|$. This result justifies the phase diagram on figure 16.

In the low–doping regime, both correlations are strongly enhanced and the low–temperature phase can be in principle a mixture of both (quasi-)long–range–orders, with the superconducting component falling to zero at half filling. The instability is in the parquet regime: the critical fluctuations are a mixture of two fluctuating channels and can not be treated by an effective mean–field theory like BCS or RPA. In other words, the parquet regime is deeply non Migdalian so that the vertex corrections are as important as the p–p loops. The vertex corrections can not be

seen as small any more but have to be taken at all orders, just as the p-p diagrams, and together with other p-h loops.

The situation is less complicated in the BCS regime. There, a low energy effective action can be constructed so that only the p-p diagrams contribute to the instability while the p-h parts (antiferromagnetic tendencies) are irrelevant. The attractive d-wave component of the Cooper amplitude in the LEEA is due to the higher energies ($\epsilon > |\mu|$) where the p-h diagrams are important. In the BCS regime only superconductivity is possible as a low-temperature order.

As we are considering a two-dimensional system, one should be careful about the interpretation of T_c : in the case of magnetism, this indicates the onset of well-defined finite-range correlations. For weak interactions, this is typically a very well-defined crossover.³⁴ In the case of pairing T_c^{RG} can be identified with the onset of quasi-long-range order. Furthermore, the line between $AF(SCd)$ and SC phases on figure 16 is only partially determined in our calculations: we only know that at temperature near T_c^{RG} , this line is close to the crossover line $T = |\mu|$, but at lower temperatures we can not say anything about its position.

It is difficult to discuss the experimental results from the point of view of our phase diagram. First of all, the one-loop renormalization-group is a weak coupling perturbative method while the interactions in the copper-oxide superconductors are moderate-to-strong. For that reason our phase diagram can be compared to the experiments only qualitatively. Furthermore, in our calculations we have neglected self-energy corrections, which are in Polchinski's formalism given by Hartree-Fock-like terms with renormalized ω - and \mathbf{q} -dependent vertices (eq. 2.30). The broadening and redistribution of the spectral weight of the quasiparticles is then determined by the dynamics of the vertex, which is irrelevant and is therefore neglected. One should however notice that at the two-loop level self-energy effects become important, as known from the one-dimensional case.¹⁵ In that sense, our T_c^{RG} should be understood as a temperature where the effects of interactions start to change strongly not only the two-particles correlations, but the single particle properties as well. For that reason it seems natural to associate the temperature T_c^{RG} to the crossover temperature T_{co} found in the cuprates. The parquet regime would then correspond roughly to the under-doped situation and the BCS regime to the over-doped regime.

The “phase” $AF(SCd)$ corresponds then to the antiferromagnetism and to the pseudo-gap regime: the antiferromagnetic correlations and the localization tendencies are there accompanied more and more with the superconducting correlations as we approach the crossover line $T = |\mu|$. We expect that the critical temperature for antiferromagnetism and for superconductivity in this regime is lower than T_c^{RG} because of the self-energy corrections. In other words, at temperature T_c^{RG} in the parquet regime, the local antiferromagnetic moments and d-wave singlets are created with finite correlation lengths. This gives rise to the pseudogap in both spin and charge responses, together with the precursors of both antiferromagnetism and d-wave superconductivity. The long-range-order between superconductivity and antiferromagnetism is perhaps absent due to the fact that both types of fluctuations are strong. That is the central idea of the $SO(5)$ models³⁷ for the high- T_c superconductivity. In that language our T_c^{RG} would play the role of the mean-field critical temperature.

In the BCS regime only the superconducting fluctuations are critical. We associate thus the phase SCd to the overdoped regime. From large N arguments^{30,22} we know that the self-energy corrections disappear as T_c/t if the Fermi surface is not nested. This is the case in the BCS regime where the nesting processes are irrelevant. Consequently,

the critical temperature in this regime is well approximated by T_c^{RG} . This is in agreement with the experiments: in the overdoped regime the crossover temperature T_{co} is equal to the critical temperature for the superconductivity. Finally, mean-field arguments³⁸ suggest that one expects an incommensurate SDW (ICSDW) only in the BCS regime and only where the imperfect nesting is still strong, i.e. not far from the crossover $T = |\mu|$. However, the precision of our calculation (we cut the Brillouin zone into up to 32 θ -patches) is not sufficient to check whether a magnetic correlation function diverges at some incommensurate wave vector. In any case, the incommensurate SDW and d-superconductivity are not in competition because they appear at different places on the Fermi surface: SCd in the corners and ICSDW on the flat parts; one thus expects their coexistence.

Altogether, the phase diagram on figure 16 has important similarities to the experimental phase diagrams. The one-loop renormalization-group, taking into account electron-electron and electron-hole processes on the same footing reveals the essence of the physics of a doped half filled band of correlated electrons.

ACKNOWLEDGMENTS

Important comments of P. Nozières are acknowledged. D. Z. thanks J. Schmalian for interesting discussions and K. H. Bennemann for his hospitality at the Institut für Theoretische Physik der Freien Universität Berlin. Laboratoire de Physique Théorique et Hautes Energies is Laboratoire associé au CNRS UMR 7589. The work of D.Z. during his stay at Institut für Theoretische Physik der Freien Universität Berlin was done in the framework of an Alexander von Humboldt fellowship.

APPENDIX A: INTERACTION $U(1, 2, 3)$ AND ITS SYMMETRIES

The most general spin-rotation invariant interaction term can be written in several ways. One way is in terms of charge-charge and spin-spin interactions

$$U_c(K_1, K_2, K_3)\bar{C}(K_2, K_4)C(K_3, K_1) + U_\sigma(K_1, K_2, K_3)\bar{\mathbf{S}}(K_2, K_4) \cdot \mathbf{S}(K_3, K_1), \quad (\text{A1})$$

where C et S_i are

$$C(K_3, K_1) \equiv \sum_\sigma \bar{\Psi}_{\sigma K_3} \Psi_{\sigma K_1} \quad ; \quad S_i(K_3, K_1) = \sum_{\sigma\sigma'} \bar{\Psi}_{\sigma K_3} \sigma_{\sigma\sigma'}^i \Psi_{\sigma' K_1}. \quad (\text{A2})$$

The summation over all three energy-momenta (K_1, K_2, K_3) is assumed and $K_4 = K_1 + K_2 - K_3$. On the other hand, the interaction can also be written as a sum of one term with equal ($\sigma = \sigma'$) and one with opposite ($\sigma = -\sigma'$) spin quantum numbers, with corresponding coupling functions named $U_{\parallel}(K_1, K_2, K_3)$ and $U_{\perp}(K_1, K_2, K_3)$:

$$U_{\parallel}(K_1, K_2, K_3)\bar{\Psi}_{\sigma K_3} \bar{\Psi}_{\sigma K_4} \Psi_{\sigma K_2} \Psi_{\sigma K_1} + U_{\perp}(K_1, K_2, K_3)\bar{\Psi}_{\sigma K_3} \bar{\Psi}_{-\sigma K_4} \Psi_{-\sigma K_2} \Psi_{\sigma K_1} \quad (\text{A3})$$

with the summation over spin indices assumed. Spin-rotation invariance allows us to write the interaction part of the action as a sum of the singlet ($|\vec{\sigma} + \vec{\sigma}'| = 0$) and triplet ($|\vec{\sigma} + \vec{\sigma}'| = \sqrt{2}$) parts:

$$\bar{s}(K_4, K_3)U^S(K_1, K_2, K_3)s(K_2, K_1) + \bar{t}_\mu(K_4, K_3)U^A(K_1, K_2, K_3)t_\mu(K_2, K_1), \quad (\text{A4})$$

where s and t_μ are the variables of annihilation of the singlet and triplet states

$$s(K_2, K_1) \equiv \frac{1}{\sqrt{2}} \sum_{\sigma} \sigma \Psi_{\sigma K_2} \Psi_{-\sigma K_1}, \quad (\text{A5})$$

$$t_0(K_2, K_1) \equiv \frac{1}{\sqrt{2}} \sum_{\sigma} \Psi_{\sigma K_2} \Psi_{-\sigma K_1} \quad ; \quad t_{\pm 1}(K_2, K_1) \equiv \Psi_{\uparrow, \downarrow K_2} \Psi_{\uparrow, \downarrow K_1}. \quad (\text{A6})$$

All coupling functions in the equations (A2,A3,A4) possess the symmetry related to momentum-exchange and time-inversion. If $\mathcal{F}(K_1, K_2, K_3, K_4)$ is a coupling function two exchange operators can be defined as

$$X\mathcal{F}(K_1, K_2, K_3, K_4) \equiv \mathcal{F}(K_2, K_1, K_3, K_4) \quad (\text{A7})$$

and

$$\bar{X}\mathcal{F}(K_1, K_2, K_3, K_4) \equiv \mathcal{F}(K_1, K_2, K_4, K_3). \quad (\text{A8})$$

The time inversion operator \mathcal{T} is

$$\mathcal{T}\mathcal{F}(K_1, K_2, K_3, K_4) \equiv \mathcal{F}(K_3, K_4, K_1, K_2). \quad (\text{A9})$$

The symmetries of the coupling function are the time inversion symmetry

$$\mathcal{T}\mathcal{F} = \mathcal{F} \quad (\text{A10})$$

and the exchange symmetry

$$X\bar{X}\mathcal{F} = \mathcal{F}. \quad (\text{A11})$$

Both symmetries can be easily checked for the coupling functions in expression (A3). We will see that all other couplings can be derived from U_{\perp} only and have the same symmetry properties upon X and \mathcal{T} operations. It is easy to see that $\bar{X}\mathcal{F} = X\mathcal{F}$ if $\mathcal{T}\mathcal{F} = \mathcal{F}$: exchanging particles 1 and 2 or particles 3 and 4 are exchanged is equivalent.

We want now to find the relations between the six coupling functions in equations (A2,A3,A4). Using the Pauli principle one gets

$$U_{\parallel} = U_c + U_{\sigma}, \quad (\text{A12})$$

$$U_{\perp} = U_c - U_{\sigma} - 2XU_{\sigma}. \quad (\text{A13})$$

Let's suppose U_c and U_{σ} to be two independent functions. We can write them in the form

$$U_c = \frac{1}{4}(2 - X)U_1 + U_2, \quad (\text{A14})$$

$$U_{\sigma} = -\frac{X}{4}U_1. \quad (\text{A15})$$

If we now choose $U_1 = U_{\perp}$ it follows from (A13) that $U_2 = 0$. It means that the most general interaction can be written in terms of a single function U_{\perp} , without losing generality. The function U_{\parallel} is also contained in U_{\perp} . Namely, from two equal-spin electrons one can build only a triplet state (antisymmetric under X) so that

$$U_{\parallel} = U^A, \quad (\text{A16})$$

while

$$U_{\perp} = U^A + U^S, \quad (A17)$$

containing the singlet and the triplet interactions. U^A and U^S can be seen as the antisymmetric and symmetric parts of the same function. This function is simply U_{\perp} .

We see that all coupling functions are contained in U_{\perp} which we call simply U or U_l to make its scale dependence explicit. One thus have

$$U_c = \frac{1}{4}(2 - X)U, \quad U_{\sigma} = -\frac{X}{4}U, \quad (A18)$$

$$U^A = U_{\parallel} = \frac{1}{2}(1 - X)U, \quad U^S = \frac{1}{2}(1 + X)U. \quad (A19)$$

The effective coupling function for the renormalization of the AF correlation function (eq. 3.16) is obtained from the spin coupling

$$V_l^{AF}(\theta_1, \theta_2) = 4U_{\sigma l}(\theta_1, \theta_2, \tilde{\theta}_1), \quad (A20)$$

where we take only the θ -dependence of the coupling functions into account. The angle $\tilde{\theta}$ is related to the angle θ in such a way that the momentum difference between the particles $\mathbf{k}(\theta)$ and $\mathbf{k}(\tilde{\theta})$ is the perfect nesting vector $(\pm\pi, \pm\pi)$. The coupling function for the CDW at $\mathbf{q} = (\pi, \pi)$ would be

$$V_l^{CDW}(\theta_1, \theta_2) = 4U_{cl}(\theta_1, \theta_2, \tilde{\theta}_1). \quad (A21)$$

¹ For a recent review, see for example M. B. Maple, cond-mat/9802202 (unpublished).

² See for example: D. Pines and Ph. Nozieres, *Quantum Liquids*, Benjamin, New York (1966), and the original works: L. D. Landau, Sov. Phys. JETP **3**, 920 (1956); ibid. **5**, 101 (1957); L. D. Landau, Sov. Phys. JETP **8**, 70 (1959).

³ D. A. Wollman *et al.*, Phys. Rev. Lett. **74**, 797 (1995); J. R. Kirtley *et al.*, Nature (London) **373**, 225 (1995); Z.-X. Shen *et al.*, Science **267**, 343 (1995); R. C. Dynes, Solid State Commun., **92**, 53 (1994); W. N. Hardy *et al.*, Phys. Rev. Lett. **70**, 3999 (1993); J. A. Martindale *et al.*, Phys. Rev. **B47**, 9155 (1993); D. J. Scalapino, Phys. Rep. **250**, 329 (1995).

⁴ M. R. Norman *et al.*, cond-mat/9710163 (unpublished).

⁵ Ch. Renner *et al.*, Phys. Rev. Lett. **80**, 149 (1997).

⁶ H. Alloul *et al.*, Bull. Am. Phys. Soc. **34**, 633 (1989); Phys. Rev. Lett **63**, 1700 (1989); W. W. Waren *et al.*, Phys. Rev. Lett **62**, 1193 (1989); M. Horvatić *et al.*, Physica (Amsterdam) **235–240C**, 1669 (1994); G. V. M. Williams *et al.*, Phys. Rev. Lett **78**, 721 (1997).

⁷ R. M. Birgenau *et al.*, Phys. Rev. B **39**, 2868 (1989); J. Rossat-Mignod *et al.*, Physica (Amsterdam) **169B**, 58 (1991);

⁸ Z.-X. Shen *et al.*, *Science* **267**, 343 (1995).

⁹ D. Jérôme and H. J. Schulz, *Adv. Phys.*, **31**, 299 (1982); D. Jérôme, in "Organic Conductors", ed. J. P. Farges (Marcel Dekker, New York, 1994), p. 405.

¹⁰ J. E. Schirber *et al.*, *Phys. Rev. B* **44**, 4666 (1991); H. Mayaffre *et al.*, *Europhys. Lett.* **28**, 205 (1994); K. Miyagawa *et al.*, *Phys. Rev. Lett.* **75**, 1174 (1995).

¹¹ J. Moser, M. Gabay, P. Auban-Senzier, D. Jérôme, K. Bechgaard, and J. M. Fabre, *Eur. Phys. J. B* **1**, 39 (1998).

¹² N. F. Berk and J. R. Schrieffer, *Phys. Rev. Lett.* **17**, 433 (1966), *Phys. Rev. B* **30**, 1408 (1966).

¹³ D. J. Scalapino, *Physics Reports* **250**, 329-365 (1995).

¹⁴ N. E. Bickers, D. J. Scalapino, and S. R. White, *Phys. Rev. Lett.* **62**, 961 (1989).

¹⁵ V. J. Emery, in "Highly conducting one dimensional solids", p. 247, eds. J. T. Devreese, R. P. Evrard and V. E. Van Doren (Plenum, New York 1979);
J. Solyom, *Adv. Phys.* **28**, 201 (1979).

¹⁶ C. Bourbonnais and L. G. Caron, *Int. J. Mod. Phys.* **5**, Nos. 6 and 7, 1033 (1991).

¹⁷ H. J. Schulz, *Europhys. Lett.* **4**, 609 (1987).

¹⁸ I. E. Dzyaloshinskii, *Sov. Phys. JETP* **66**, 848 (1988).

¹⁹ I. E. Dzyaloshinskii and V. M. Yakovenko, *Sov. Phys. JETP* **67**, 844 (1988).

²⁰ A. T. Zheleznyak, V. M. Yakovenko, and I. E. Dzyaloshinskii, *Phys. Rev. B* **55**, 3200 (1997).

²¹ F. Vistulo de Abreu and B. Douçot, *Europhys. Lett.* **38**, 533 (1997).

²² D. Zanchi and H. J. Schulz, *Phys. Rev. B* **54**, 9509 (1996).

²³ D. Zanchi and H. J. Schulz, *Z. Phys. B* **103**, 339 (1997).

²⁴ J. Gonzalez, F. Guinea, M. A. H. Vozmediano, *Phys. Rev. Lett.* **79**, 3514 (1997).

²⁵ J. Ruwalds *et al.*, *Phys. Rev. B* **51**, 3797 (1995).

²⁶ H.-J. Kwon, *Phys. Rev. B* **55**, 9788 (1997).

²⁷ Hsiu-Hau Lin, Leon Balents, and Matthew P. A. Fisher, *Phys. Rev. B* **56**, 6569 (1997).

²⁸ W. Fettes and I. Morgestern, *cond-mat/9801227* (unpublished).

²⁹ Shiwei Zhang, J. Carlson, and J. E. Gubernatis, *Phys. Rev. Lett.* **78**, 4486 (1997).

³⁰ R. Shankar, *Rev. Mod. Phys.* **66**, 129 (1994).

³¹ J. Polchinski, Nucl. Phys. **B231**, 269 (1984).

³² Tim R. Morris, Int. Jour. Mod. Phys. **A**, Vol. 9, No. 14, 2411 (1994).

³³ J. W. Negele and H. Orland, “Quantum Many-Particle Physics”, Addison Wesley (1988).

³⁴ H. J. Schulz, Phys. Rev. B **39**, 2940 (1989).

³⁵ E. Fradkin, “Field Theories of Condensed Matter Systems”, Addison Wesley (1991).

³⁶ S. Weinberg, Nucl. Phys. **B413**, 567 (1994).

³⁷ S.-C. Zhang, Science **275**, 1089 (1997).

³⁸ D. Zanchi, Ph.D. thesis, Université Paris-Sud (1996) (unpublished).